HARDWARE FOR IMPEDANCE CARDIOGRAPHY

A dissertation
submitted in partial fulfillment of the requirements
for the degree of

Master of Technology

by

S. Navaneetha Krishnan Naidu

(Roll No. 03330001)

under the supervision of

Prof. P. C. Pandey

Biomedical Engineering Group
School of Biosciences and Bioengineering
Indian Institute of Technology, Bombay

July 2005

INDIAN INSTITUTE OF TECHNOLOGY, BOMBAY

M. Tech. Dissertation Approval

Dissertation entitled, "*Hardware for Impedance Cardiography*", submitted by *S. Navaneetha Krishnan Naidu (Roll No. 03330001)* is approved for the award of degree of *Master of Technology in Biomedical Engineering*.

Supervisor : _____ (Prof. P. C. Pandey)

Internal examiner : _____ (Prof. S. Mukherji)

External examiner : _____ (Prof. L. R. Subramanyan)

Chairman : _____ (Prof. T. S. Rathore)

Date: July 11, 2005

ACKNOWLEDGEMENTS

I would like to thank Prof. P. C. Pandey for giving me an opportunity to work on this project and for his guidance, support, and encouragement throughout the course of this project. I am also thankful to Prof. S. Mukherji for his suggestions during the presentations.

I would like to thank Mr. Vinod K. Pandey for his helpful suggestions and the useful discussions I had with him. I would also like to thank Mr. Vidyadhar Kamble for his help in the lab and PCB fabrication and Mr. Dinesh S. Choudhary and Ms. Syrpailyne Wankhar for their help in PCB designing. My thanks are also due to Mr. Rajesh Gawai for making the casing for the thoracic impedance simulator. I would also like to thank all my friends in the lab for their help during the course of the project.

July 2005 **S. Navaneetha Krishnan Naidu**

S. Navaneetha Krishnan Naidu / Prof. P. C. Pandey (supervisor): “Hardware for impedance cardiography”, *M. Tech. Dissertation*, Biomedical Engineering Group, School of Biosciences and Bioengineering, Indian Institute of Technology, Bombay, July 2005.

ABSTRACT

Impedance cardiography is a non-invasive technique for measuring cardiac stroke volume and diagnosing various cardiac disorders. The thoracic impedance varies during the cardiac cycle with the variation in amount of blood. This impedance change is detected by injecting a high frequency (20 – 400 kHz), low intensity (<5 mA) current through a pair of injecting electrodes and sensing the resultant amplitude modulated signal across the thorax through another pair of sensing electrodes. This amplitude modulated signal is demodulated and processed to obtain the cardiac stroke volume. The objective is to improve the hardware modules of the existing instrument for better performance. The oscillator module has been modified for improved short term amplitude stability. The demodulation scheme has been changed from a precision rectifier based one to a vector lock-in amplifier based demodulation. The parameters of the baseline restoration circuit have been modified for better performance. The existing thoracic impedance simulator has been modified to a compact microcontroller based circuit, to reduce internal wiring, and better user interface.

CONTENTS

LIST OF SYMBOLS

Symbol	Explanation
Ca^{2+}	Calcium ion
K^{+}	Potassium ion
ρ	Resistivity
Z_o	Impedance of the fixed conduction volume
Z_N	Impedance of changing volume
$Z(t)$	Net impedance
$z(t)$	Varying impedance
L	Length of the column
A	Cross-sectional area of the column
v	Volume of the column
ΔV	Volume change of the small parallel column
ΔZ	Impedance change across the column
$-(dz/dt)_{max}$	Most negative (upward in the graph) deflection during systole measured from zero.
T_{lvet}	Left ventricular ejection time
$-dz/dt$	Impedance cardiogram
β	Negative feedback gain
A	Forward gain of the amplifier
L_-	Negative amplitude limit
L_+	Positive amplitude limit
Vp	Carrier signal
Vq	90° phase shifted version of the carrier, Vq
$p(t)$	in-phase component of the modulating signal
$q(t)$	quadrature component of the modulating signal

LIST OF ABBREVIATIONS

Symbol	Explanation
ECG	Electrocardiogram
ICG	Impedance cardiogram
SV	Stroke volume
DC	Direct current
AV	Atrio-ventricular
SA	Sino-atrial
EDV	End diastolic volume
ESV	End systolic volume
SV	Stroke volume
CO	Cardiac output
HR	Heart rate
PCG	Phono cardiogram
JFET	Junction field effect transistor
SUT	System under test
AC	Alternating current
ADC	Analog-to-digital converter
DAC	Digital-to-analog convertor
PWM	Pulse width modulation
PCB	Printed circuit board
LCD	Liquid crystal display
CM	Common mode
DM	Differential mode

LIST OF FIGURES

LIST OF TABLES

Chapter 1
INTRODUCTION

1.1 Background

The electrical activity of the heart can be monitored by investigating the electrocardiogram (ECG). But the main action of the heart is mechanical pumping of blood. Impedance cardiography is a technique which allows non-invasive monitoring of this mechanical action of the heart. It involves injecting a high frequency low intensity current into the thorax through a pair of electrodes. Voltage developed across a pair of sensing electrodes gets amplitude modulated because of variation in the thoracic impedance due to changing blood volume. The variation in the impedance is sensed and used for calculating the stroke volume (SV) *i.e.*, the amount of blood pumped by the heart per heartbeat and other diagnostic information. Compared to other techniques, impedance cardiography is non-invasive, easy to apply and lower in cost.

1.2 Project objective

This project involves modification of the hardware used for the existing impedance cardiograph instrument for better performance. It is a continuation of earlier work done at IIT Bombay. The analog part of the instrument consists of an oscillator, a voltage-to-current converter for current excitation of the thorax, voltage sense amplifier, demodulator and baseline restoration circuit. The sections which need to be modified include the oscillator section whose short term amplitude stability needs to be improved, the demodulator section where the performance at the frequency used (100 kHz) is not satisfactory and the modification of the parameters of the baseline restoration circuit for optimum use of the ADC dynamic input range.

A new oscillator has been implemented whose short term amplitude stability is much better. The demodulation technique has been changed. Vector lock-in amplifier

technique has been used for demodulator, and it has better noise rejection characteristics. The baseline restoration circuit has been modified as required.

A thoracic impedance simulator, for testing and calibration of impedance cardiograph has been developed as an upgradation of earlier design. It has a LCD display and two soft keys for user interaction. It has provision for variation of heart rate, basal impedance, change in impedance and amplitude of ECG common mode and differential mode signals.

1.3 Dissertation outline

Chapter 2 reviews the basics of impedance cardiography. The third chapter gives the block description of the existing instrument. The hardware modifications implemented in the impedance cardiograph instrument is reported in the fourth chapter. The fifth chapter gives details about the design of the thoracic impedance simulator. The sixth chapter presents a summary of the work and gives suggestions for future work.

Chapter 2

BASICS OF IMPEDANCE CARDIOGRAPHY

2.1 Anatomy of the heart

The heart consists of four chambers: left atrium, left ventricle, right atrium, and right ventricle, as shown in Fig. 2.1 [1][2][3]. The left atrium and ventricle are separated by the mitral valve. The right atrium and right ventricle are separated by the tricuspid valve. The valves between the atrium and the ventricle are also known as atrio-ventricular (A-V) valves. The pulmonic valve is situated between the right ventricle and the pulmonary artery and the aortic valve between the left ventricle and the aorta. The deoxygenated blood (blood poor in oxygen content) from all peripheral organs of the

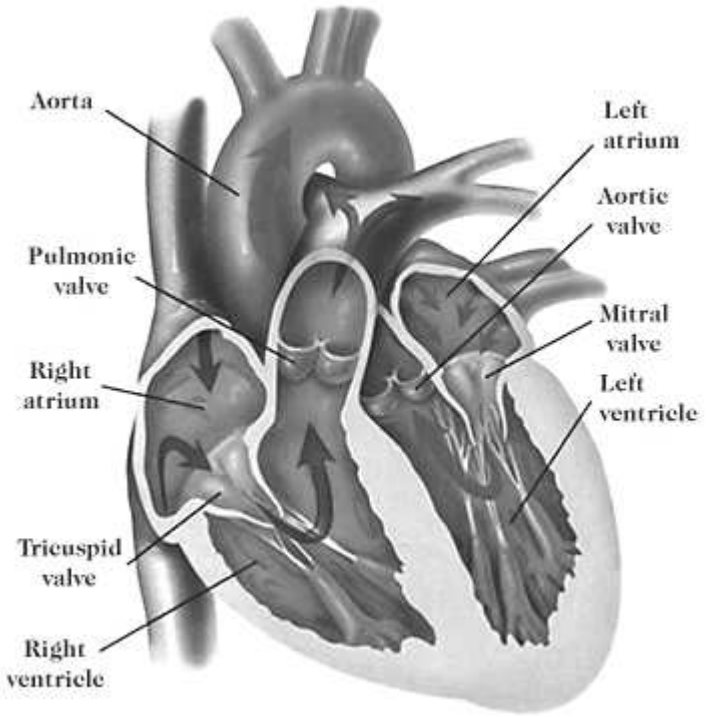

Fig. 2.1 The chambers of the heart and blood vessels [3].

body flow into the right atrium. The right atrium pumps it to the right ventricle, from where it is pumped to the lungs through pulmonary arteries for oxygenation. From the lungs, the blood arrives to the left atrium through pulmonary veins. The left atrium pumps the oxygenated blood to the left ventricle which in turn pumps it to the peripheral organs through the aorta, completing the blood circulation. The mechanical activity of the heart is actually caused by the electrical activity of the cardiac muscle cells. Each cycle is initiated by spontaneous generation of an action potential in the sino-atrial (SA) node located in the anterior wall of the right atrium. These potentials travel through both atria to the A-V node, located between the atria and ventricles, and then to the ventricles.

2.2 The cardiac cycle

A cardiac cycle consists of a systole and diastole of both atria plus a systole and diastole of both ventricles. As a chamber of the heart contracts, the pressure of the fluid within it increases. Due to this, pressure changes occur and blood flows from areas of higher blood pressure to areas of lower blood pressure as shown in Fig. 2.2. The cardiac cycle can be divided into three phases: diastole or relaxation, ventricular filling, and ventricular systole.

In the relaxation phase, all four chambers are in diastole at the end of a heartbeat. As the ventricles relax, pressure within the chambers drops and blood starts to flow from the pulmonary trunk and aorta back towards the ventricles. As the pressure drops below the aortic pressure, the aortic valves close. There is a brief interval when the ventricular blood volume does not change because both A-V valves and aortic and pulmonic valves are closed. This period is called isovolumic relaxation. As the ventricles relax, the space inside expands and the pressure falls rapidly. When ventricular pressure falls below atrial pressure, the A-V valves open and ventricular filling begins.

As soon as the A-V valves open, there is a large amount of blood flow which had accumulated in the atria during the time the ventricles were contracting. The firing of the SA node results in atrial depolarization which is followed by atrial contraction after some time. At the end of ventricular diastole, there is about 130 ml of blood in each ventricle which is known as end-diastolic volume (EDV).

The impulse from the SA node after passing through the A-V node reaches the ventricles causing them to depolarize. Ventricular contraction begins and blood is pushed

up against the A-V valves forcing them shut. As ventricular contraction continues, the pressure inside rises rapidly. For about 0.05 s, all four valves are closed again. This period is called isovolumic contraction. When left ventricular pressure surpasses aortic pressure and right ventricular pressure rises above the pressure in the pulmonary trunk, both aortic and pulmonic valves open and ejection of blood begins and continues until the ventricles start to relax. Then the aortic and pulmonic valves close and another relaxation period begins. The volume of blood still left in each ventricle after ventricular systole is known as end-systolic volume (ESV). At rest, it is about 60 ml.

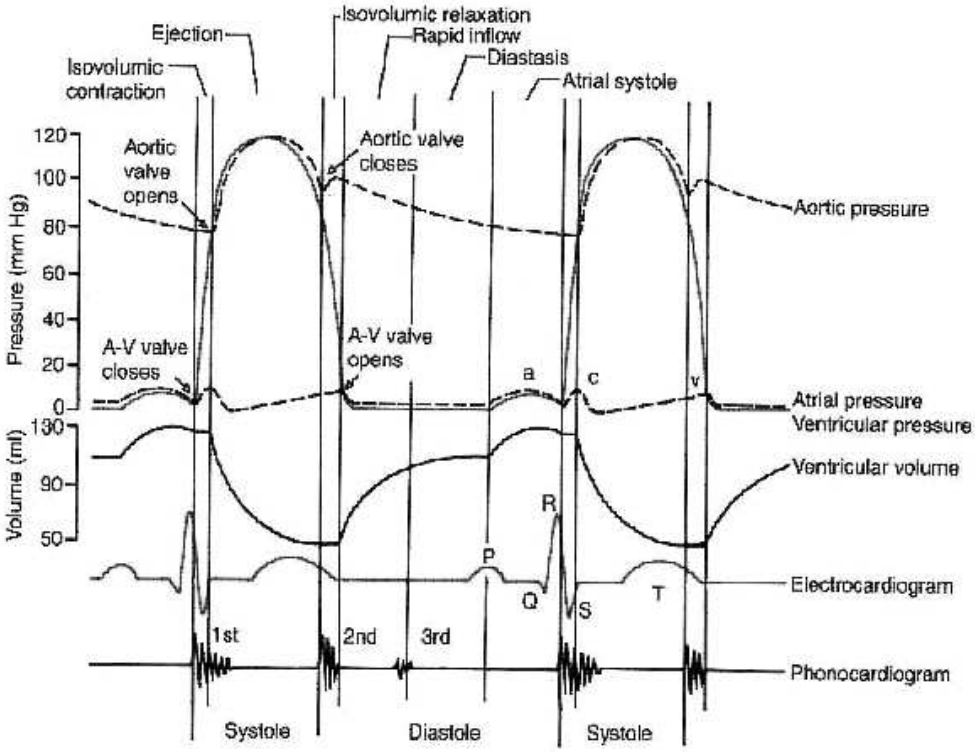

Fig. 2.2 The cardiac cycle [1].

During each cardiac cycle, four heart sounds are generated. In a normal heart, however, only the first two are loud enough to be heard by stethoscope. The first heart sound, which can be described as "lubb", is the sound created by blood turbulence associated with closure of the A-V valves soon after ventricular systole begins. The second heart sound, which can be described as "dub", is the sound created by blood turbulence associated with closure of the aortic and pulmonic valves at the beginning of ventricular diastole.

2.3 Cardiac output

The volume of blood ejected by the ventricle with each contraction is known as stroke volume (SV). Cardiac output (CO) is the amount of blood ejected from the left ventricle (or the right ventricle) into the aorta (or pulmonary trunk) each minute. Thus, cardiac output is SV times the heart rate (HR), the number of heartbeats per minute. In a typical resting adult, the stroke volume averages 70 ml/beat and heart rate is about 72 beats/min. This gives an average CO of 5.04 litres/min.

Stroke volume is the difference between the end-diastolic volume (EDV) and end-systolic volume (ESV). Three important factors regulate stroke volume in different circumstances: preload, contractility and afterload.

Preload: This refers to the amount of stretch on cardiac muscle fibres just before they contract. According to Frank-Starling law of the heart [1], the more the heart is filled during diastole, the greater the force of contraction during systole *i.e.*, the greater the EDV, the more forceful the contraction. EDV is determined by two factors: duration of ventricular diastole and venous pressure. When heart rate increases, the duration of diastole is shorter. Less filling time means a smaller EDV and the ventricles may contract before they are adequately filled. When the venous pressure increases, the amount of blood forced into the ventricles increases and EDV increases.

Contractility: This is the strength of contraction of the ventricular muscles at any given preload. Substances that increase contractility are called positive inotropic agents and those that decrease contractility are called negative inotropic agents. Thus, for a given preload, the stroke volume is larger when a positive inotropic substance is present. Positive inotropic agents promote Ca^{2+} inflow during cardiac action potentials which strengthens the force of the subsequent muscle fibre contraction. They include stimulation of the sympathetic division of the autonomic nervous system, hormones such as epinephrine and norepinephrine, increased Ca^{2+} level in the extracellular fluid, and the drug digitalis. Negative inotropic agents include inhibition of the sympathetic division of the autonomic nervous system, anoxia, acidosis, some anesthetics, and increased K^{+} level in the extracellular fluid.

Afterload: This refers to the pressure that must be exceeded before ejection of blood from the ventricles can begin *i.e.*, the pressure that must be overcome before the semilunar valves can open. When afterload increases, the stroke volume decreases.

Afterload can increase when blood pressure is elevated or arteries are narrowed by atherosclerosis.

2.4 Basis for impedance cardiography

The resistivity of blood is lesser than that of other body tissues [4][5]. Thus when the volume of blood in the thoracic cavity increases, the impedance of the thorax decreases. The typical values of resistivity of biological materials [4] is given in Table 2.1.

Table 2.1 Resistivity of biological materials [4].

Material	**Resistivity (ρ), Ω.cm**
Blood	150
Plasma	63
Cardiac muscle	750
Lung	1275
Fat	2500

In impedance cardiography, a high frequency (20 – 400 kHz) low amplitude (<5 mA) current is passed through the thorax [4][5]. During systole, when the volume of blood in the thorax increases, the impedance falls. The corresponding voltage drop is recorded which is thus proportional to the stroke volume.

An impedance model for the thorax was proposed by Kubicek and a formula for stroke volume calculation was derived by him from the model [6][7]. The model known as parallel column model consists of two parallel columns of conducting material as shown in Fig. 2.3, one with a constant impedance Z_o and other with a variable impedance Z_N. The net impedance is given by

$$Z(t) = Z_o \parallel Z_N \tag{2.1}$$

If the cross sectional area of the column "N" varies from zero to a finite value the change in impedance across the parallel column is given by

$$z(t) = Z(t) - Z_o$$

$$z(t) = -\frac{{Z_o}^2}{(Z_o + Z_N)} \tag{2.2}$$

Since $z(t) << Z_o$ we can assume $Z_N >> Z_o$,

$$z(t) = -\frac{Z_o^{\,2}}{Z_N} \tag{2.3}$$

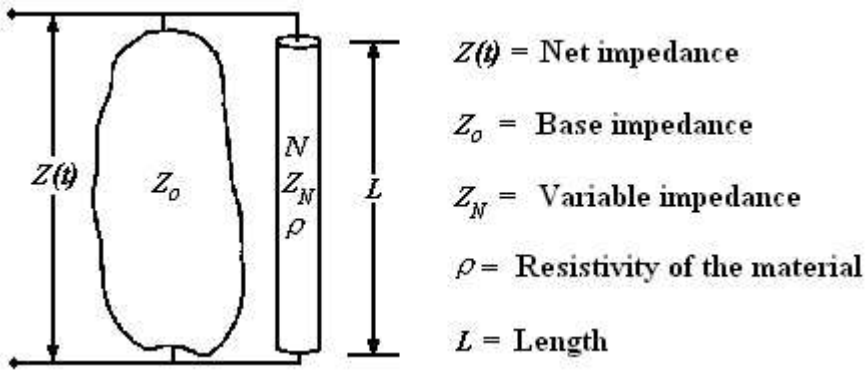

Fig. 2.3 Parallel column model [7].

Considering Z_N to be a cylinder with length, *L*, cross-sectional area, *A*, and volume $v = LA$, Z_N is given by

$$Z_N = \frac{\rho L^2}{v} \tag{2.4}$$

where, ρ is the resistivity of the material.

Hence the impedance variation can be given as

$$z(t) = -\frac{Z_o^{\,2} v}{\rho L^2} \tag{2.5}$$

An assumption was made that the inflow of blood into the lungs is the source of impedance change and the volume of the column N is zero before systole. So during systole, the impedance starts decreasing and assuming no blood leaves the lungs during systole, the maximum impedance change can be written as

$$\Delta Z = (-z)_{\max}$$

The change in volume of the column can be written as

$$\Delta V = \rho \frac{L^2}{Z_o^{\,2}} \Delta Z \qquad (2.6)$$

where,

ΔV is the volume change of the small parallel column

Z_o is the impedance of the fixed conduction volume

ΔZ is the impedance change across the column

The outflow of blood from the lungs into the heart was not accounted during systole.Later a correction was made [6][7], in which the extrapolation technique shown in Fig 2.4,

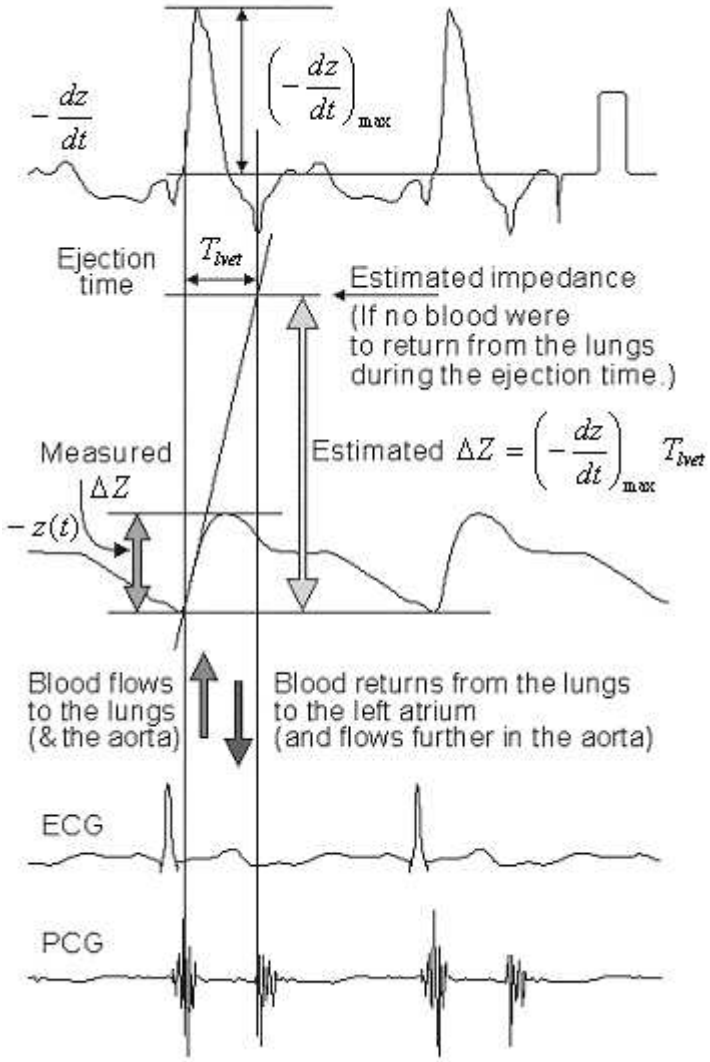

Fig. 2.4 Stroke volume calculation by extrapolation technique [6].

was introduced to account for the outflow of blood from the lungs into the heart in the later part of systole. This is as given below

$$\Delta V = \frac{\rho L^2}{Z_o{}^2}\left(-\frac{dz}{dt}\right)_{\max} T_{lvet} \qquad (2.7)$$

where, $\left(-\frac{dz}{dt}\right)_{\max}$ is the most negative (upward in the graph) deflection during systole measured from zero, and T_{lvet} is the left ventricular ejection time (time between the first heart sound "B" and aortic valve closure "X") as shown in Fig. 2.5. A number of other refinements have been reported [8][9].

2.5 Impedance cardiogram

A typical impedance cardiogram is shown in Fig. 2.5. The impedance variation signal is *z(t)* waveform. It is customary to plot -*z*(*t*), because an increase (positive deflection) in this waveform is related to increase in the volume of blood. The derivative of this waveform, -*dz*/*dt* is termed as the impedance cardiogram, and is used for calculation of stroke volume, as well as for obtaining diagnostic information. The ECG waveform is used as a reference for the 'R' point. The PCG is used as a reference to note the heart sounds.

Various points on the -*dz/dt* waveform have been identified to correspond to the following physiological events:

A: Atrial contraction
B: Closure of tricuspid valve
X: Closure of aortic valve
Y: Closure of pulmonic valve
O: Opening snap of mitral valve
Z: Third heart sound

The contribution of cardiovascular system to the impedance signal is a sum of two components [8]:

1. Plethysmographic component – The contraction of the ventricles causes the pressure in aorta to change which in turn causes the volume of the aorta to change leading to the impedance change.

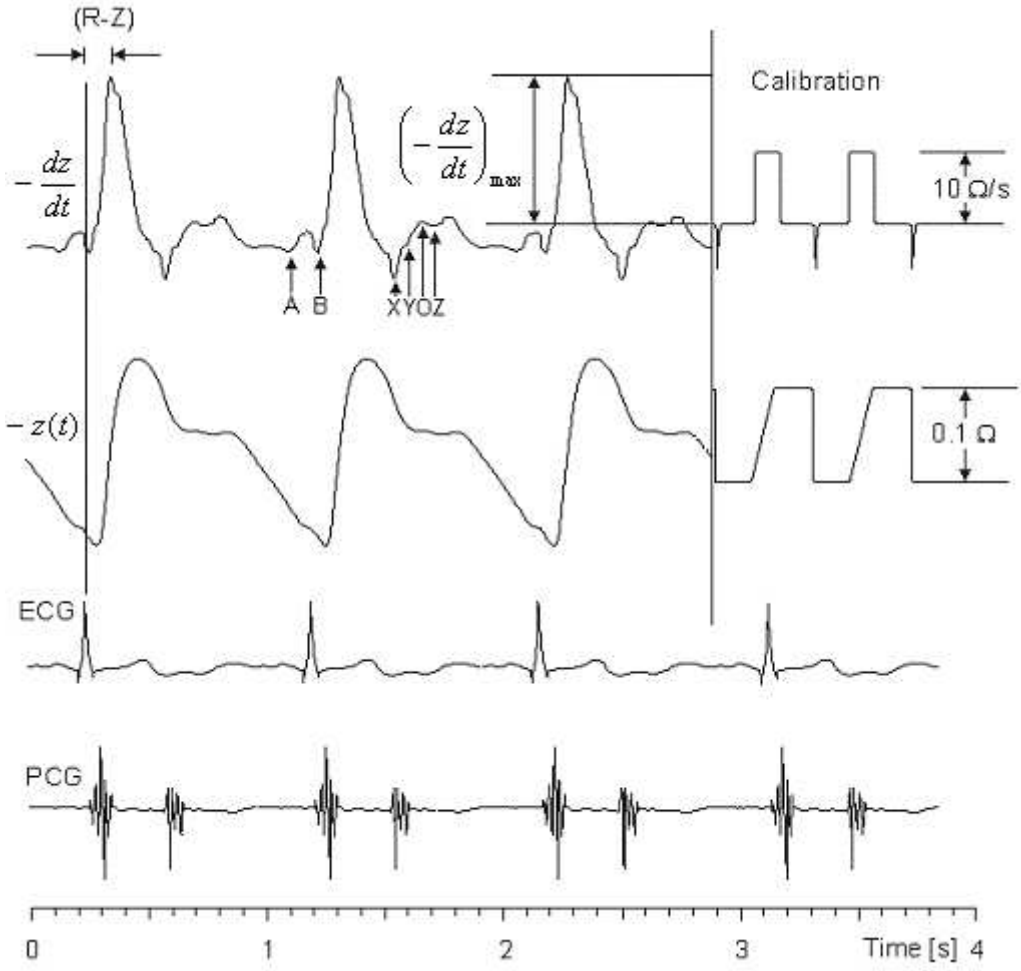

Fig. 2.5 Typical impedance cardiography related waveforms -*z*(*t*) and -*dz*/*dt*, along with ECG and PCG [6].

2. Erythrocyte-orientation component – At the end of diastole, the erythrocytes are randomly oriented within the plasma. The current lines have an extended path-length and the resistivity of blood is high. During systole, the erythrocytes become aligned with their plane parallel to the main axis of the aorta. As the velocity increases, the percentage of aligned erythrocytes increases thus, the conductivity of flowing blood is higher than that of stationary blood.

The heart itself does not significantly contribute to the impedance signal due to the following reasons:

1. The physical volume of the heart represents 10% of the total volume of the thorax and its conductivity is totally shielded by the aorta and the vena cava.
2. During systole, the heart is expelling blood decreasing its conductivity while the conductivity of the blood vessels is increasing due to the inflow of blood into them.

2.6 Earlier work

Several impedance cardiographs have been developed around the world [7][10–15]. Many instruments have become commercially available. Information on some of these instruments is given in Appendix A.

Work on impedance cardiography has been carried out at IIT Bombay from 1990 onwards. An instrument for measuring the cardiac output and stroke volume was developed by Joshi in 1993 [16][17]. In 1997, Patwardhan developed a software for off-line display of all the recorded physiological signals and also developed a thoracic impedance simulator for calibration of the impedance cardiograph [18]. Kuriakose in 2000 modified the circuit to improve the sensitivity and consistency of the instrument [19]. Later Manigandan in 2004 improved the instrument further, particularly by implementing a microcontroller based drift cancellation circuit and improving the thoracic impedance simulator [20].

Chapter 3

IMPEDANCE CARDIOGRAPH

3.1 Block diagram

Earlier work carried out at IIT Bombay for impedance cardiography [18][19][20] has resulted in a prototype instrument. The block diagram of the instrument is as shown in Fig. 3.1 which is basically based on the design used by Qu *et al.* [21][22]. The various blocks are explained below.

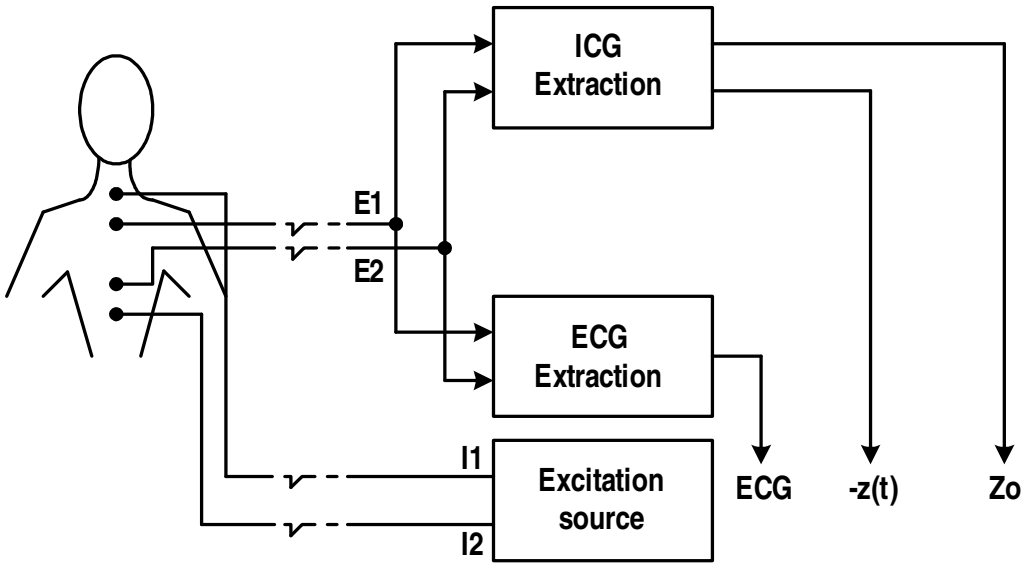

Fig. 3.1 Block diagram of the ICG instrument along with placement of electrodes based on [20].

Excitation circuit

The excitation circuit consists of a Wein bridge oscillator and a voltage-to-current converter. The Wein bridge oscillator produces a sinusoidal waveform of 100 kHz frequency. There is a buffer stage to improve the stability of the oscillator. There are two options for the voltage-to-current converter: unbalanced and balanced. In the unbalanced one, one of the current injection points is at virtual ground and the output voltage is developed at the other end. In the balanced one, the two current injection points are

maintained at 180° phase. High impedance indicator circuit indicates whether the contacts of the electrodes with the body are proper or not.

ICG and ECG extraction circuits

The two voltage sensing electrodes are connected to the ICG extraction circuit. It consists of an instrumentation amplifier with bandpass filter, demodulator, averager for Z_o and baseline restoration circuit for -$z(t)$. The instrumentation amplifier amplifies the signal obtained and has a 16 kHz high pass filter at the input to remove power line interference, ECG and other motion artifacts. The demodulator section consists of a full wave precision rectifier followed by a low pass filter. The signal obtained is again low pass filtered to obtain Z_o. A microcontroller based baseline restoration circuit is used to remove respiration artifacts to obtain -$z(t)$. The pair of voltage sensing electrodes are also connected to ECG extraction circuit which has an instrumentation amplifier and a low pass filter to get ECG. This ECG is obtained from two sensing electrodes on the chest and is different from the signals obtained using standard leads. The ECG is primarily for use as timing reference for processing of the ICG waveform, and not meant for any diagnostic information itself. Provision for obtaining ECG from limb electrode configuration has also been provided.

3.2 Software signal processing

The signals, -$z(t)$, Z_o, ECG, and phonocardiogram (PCG) are acquired using a USB-based data acquisition unit. The PCG signal is obtained from a separate phonocardiograph. The signals are processed using filters, the required parameters according to the formula for SV are evaluated and the SV calculated. The signal processing is done in MATLAB [23]. Most of the motion artifacts fall in the range of the frequency range of -$z(t)$ and thus filtering cannot be done to remove them. In this case, ensemble averaging can be used with the R points of the ECG waveform providing as fiducial marks.

3.3 Electrodes

There are two possible kinds of electrode configurations possible: two-electrode and four-electrode. A four-electrode configuration of electrodes is used, wherein; two

outer electrodes inject current while two inner electrodes detect the voltage. In a two-electrode configuration, the two electrodes injecting current also measure the voltage. This can lead to errors because of voltage drops across the skin-electrode contact impedance [24]. This is eliminated in a four electrode configuration. Suction cup stainless steel electrodes are used for the current injecting electrodes and pre-gelled disposable Ag-AgCl ECG electrodes are used as the sensing electrodes. Gel is applied between the electrode and the skin at the skin-electrode interface to obtain a good contact.

The main sources of interference in ICG are from respiration and body movements. Respiration causes changes in the amount of air in the thorax and movement of the thorax which leads to changes in the impedance. The changes in the orientations and locations of the internal body parts during movements also contribute to noise by changing the distribution of current in the body segment. Electrodes are placed in the central area of the body where body movements cause minimal displacement of the electrodes. They are also located in the area which is the largest contributor to the impedance signal.

3.4 Hardware modifications needed

The short term amplitude stability of the oscillator has to be studied and brought down. The precision rectifier used for amplitude demodulation does not perform well at the frequency used (100 kHz). Therefore this section needs to be modified by changing the components in the existing circuit or by going in for a different demodulation scheme. The baseline restoration circuit has to be modified for optimum use of the ADC dynamic input range.

Chapter 4
HARDWARE MODIFICATION

4.1 Introduction

As mentioned in Section 3.4, in the existing prototype developed in the lab [18][19][20], the hardware sections requiring improvement are: signal source, demodulator, and baseline restoration circuit. For this purpose, the performance of existing circuits was analyzed, alternatives evaluated, and a modified or new version of the circuit was finalized. This chapter presents these modifications.

4.2 Signal source

The short term amplitude stability of the signal source is important because this gets amplitude modulated due to impedance variation. If the amplitude is not stable, then after demodulation this variation in amplitude would get reflected in the output signals. Use of direct digital synthesis for excitation source has been earlier reported [25]. It was decided to first study the performance of the Wein bridge oscillator circuit in the existing instrument, try out modifications, and work out alternatives.

4.2.1 Wein bridge oscillator

The existing instrument uses Wein bridge oscillator as the voltage source for the V-I converter driving the current electrodes as shown in Fig. 4.1. It was modified to increase its short term stability [26][27] as shown in Fig. 4.2. The amplitude stabilization of the oscillator has been obtained with the help of a JFET, Q_1, used as a voltage-variable resistance [26]. At power-up, the JFET has minimum resistance because its gate voltage is zero. This allows the oscillations to build up as the gain is high. The negative peak value of the output sinusoidal waveform after it crosses the voltage drops across the two diodes is detected by C_3 and R_5 and is applied to the gate of the JFET as V_{gs}. As V_{gs} goes

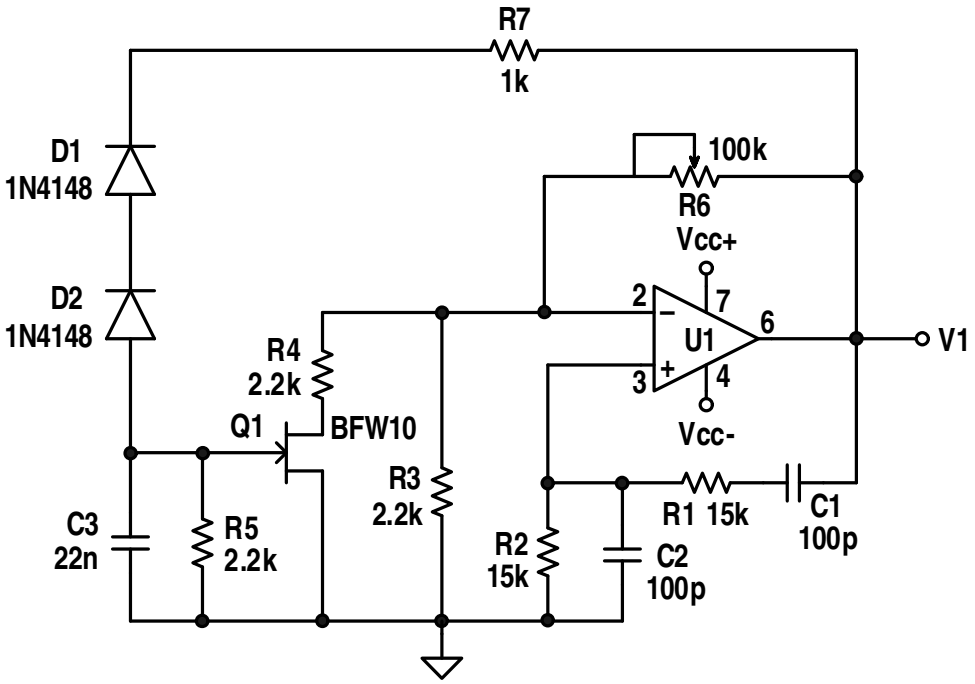

Fig. 4.1 Wein bridge oscillator used by Manigandan [20] (U1: LF356).

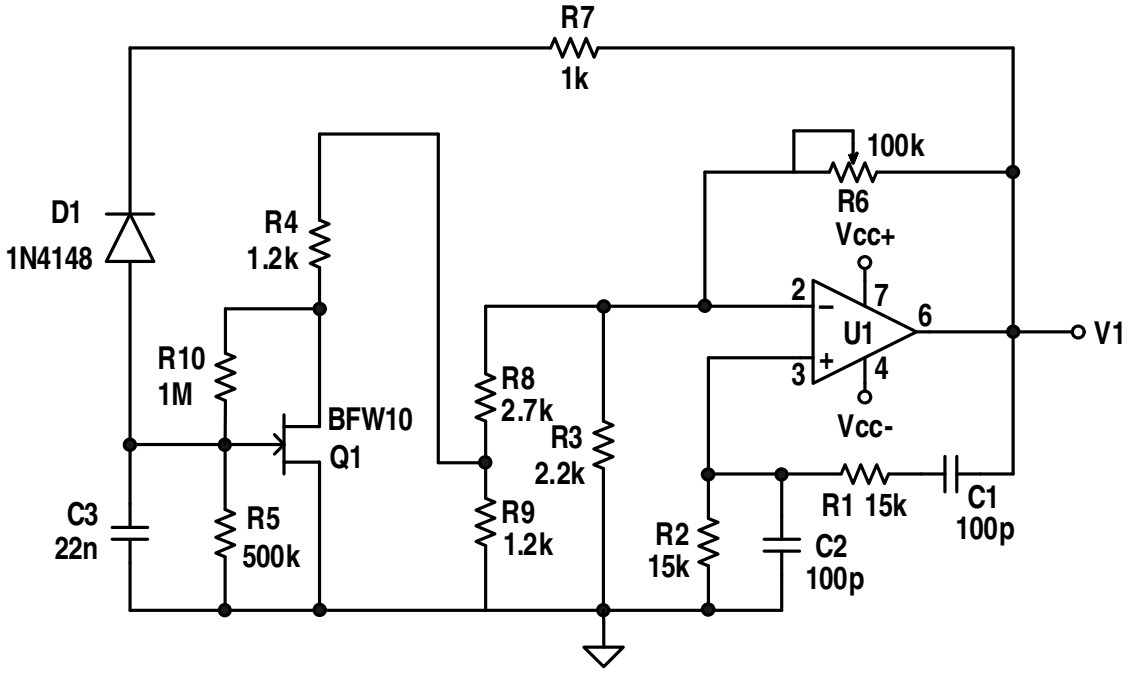

Fig. 4.2 Wein bridge oscillator with modified amplitude stabilization (U1: LF356).

more negative, the JFET channel width decreases and the drain-to-source resistance, r_{ds} increases. In the oscillator, the JFET resistance, r_{ds} is used in parallel with R_3. Thus if the

output peak value of the sinusoidal waveform is less, r_{ds} is low and the gain of the feedback amplifier is more than that 3 ,*i.e.*, more than that is required for oscillation to be sustained. Thus, the peak of the output voltage starts increasing. This increases r_{ds} which in turn reduces the gain of the amplifier. Thus with time, a stable point is reached where sustained oscillations are obtained.

The problem of amplitude instability has been found to be the result of operating the JFET at relatively large V_{ds}. The observed value of V_{ds} was around 5 V p-p. Thus, this problem of short term stability can be reduced by reducing the V_{ds} of the JFET. This has been done with a resistive voltage divider formed by resistors R_8 and R_9, placed at the inverting input of the op amp dividing V_{ds} by a factor of three. The ac characteristics of the JFET is linearized by superimposing one half of the drain–source voltage on the gate-source control voltage by resistors R_5 and R_{10} [27]. The two diodes were used to subtract the two knee voltages from the output waveform. Since the knee voltages may vary for the diodes, the two diodes were replaced by one. The rapid variation in the earlier design has been brought down in the new one. The output stability can be increased further by a diode limiter circuit at the output, but it will introduce distortions, which can be reduced by filtering the output.

4.2.2 Quadrature oscillator

It was further decided to use vector lock-in amplifier with synchronous detection for the demodulation. This requires the oscillator section to generate output sinusoidal waveforms having a phase difference of 90^o between them. After evaluating the various quadrature oscillator circuits, it was decided to use Bubba oscillator [28][29]. The oscillator was assembled to study its short term amplitude stability. It is basically a phase shift oscillator with four RC sections providing phase shifts of 45^o and an inverting amplifier providing the required 180^o phase shift for oscillations as shown in Fig. 4.3 [29]. The outputs taken at alternate points along the RC chain give sinusoidal waveforms with a phase shift of 90^o between each other.

At a phase shift of 45^o, attenuation due to each RC network is equal to 0.707 times the output of the preceding stage. Thus, the output after the four RC sections is equal to $(0.707)^4$ times the output of the inverting amplifier which is the β of the circuit.

i.e., $\beta = (0.707)^4 = 0.2498$

For oscillations, the gain of the inverting amplifier should be at least $1/(0.707)^4$, *i.e.*,

$A\beta \geq 1$, for oscillations

$\therefore A \geq 4.0024$

In the circuit, the R_1, C_1, R_2, C_2, R_3, C_3, R_4 and C_4 provide the phase shifts. A_2, A_3 and A_4 are non-inverting buffers. A_1 forms the inverting amplifier with the gain decided by R_1 and R_2. A limiter circuit has also been implemented with A_1 with diodes D_1 and D_2, and R_7 to R_{10}. The negative and positive limits are given by Eqn. 4.1 and 4.2

$$L_- = -0.7\left(1 + \frac{R_8}{R_7}\right) - V_{CC-}\frac{R_8}{R_7} \tag{4.1}$$

$$L_+ = 0.7\left(1 + \frac{R_9}{R_{10}}\right) + V_{CC+}\frac{R_9}{R_{10}} \tag{4.2}$$

Since the RC networks reduce the magnitude, the second sinusoidal waveform would have to be amplified to the same level as the first. But since the limiting used is of soft type, if the amplitude of one output is increased, the other would also increase. So, a separate non-inverting amplifier has to be used for the second output. A_2, A_3 and A_4 has been implemented with a TL084 quad op amp and A1 has been implemented with LF356.

The output frequency is given by

$$f = \frac{1}{2\pi RC}$$

Taking R = 15 kΩ and C = 100 pF, the nominal frequency is 106 kHz. The output frequency was found to be 82 kHz. The amplitudes of the two outputs were observed to be 6.0 V_{pp} and 6.25 V_{pp}.

The amplitude stability of the earlier Wein bridge oscillator, the modified Wein bridge oscillator, and Bubba oscillator were measured using a DSO manufactured by Tektronix (model: TDS 5054). For comparison, the measurements were also done on the output from an arbitrary waveform generator, HP33120A. The test results are given in Table 4.1. It can be seen that Bubba oscillator has the highest amplitude stability and it has been decided to be used.

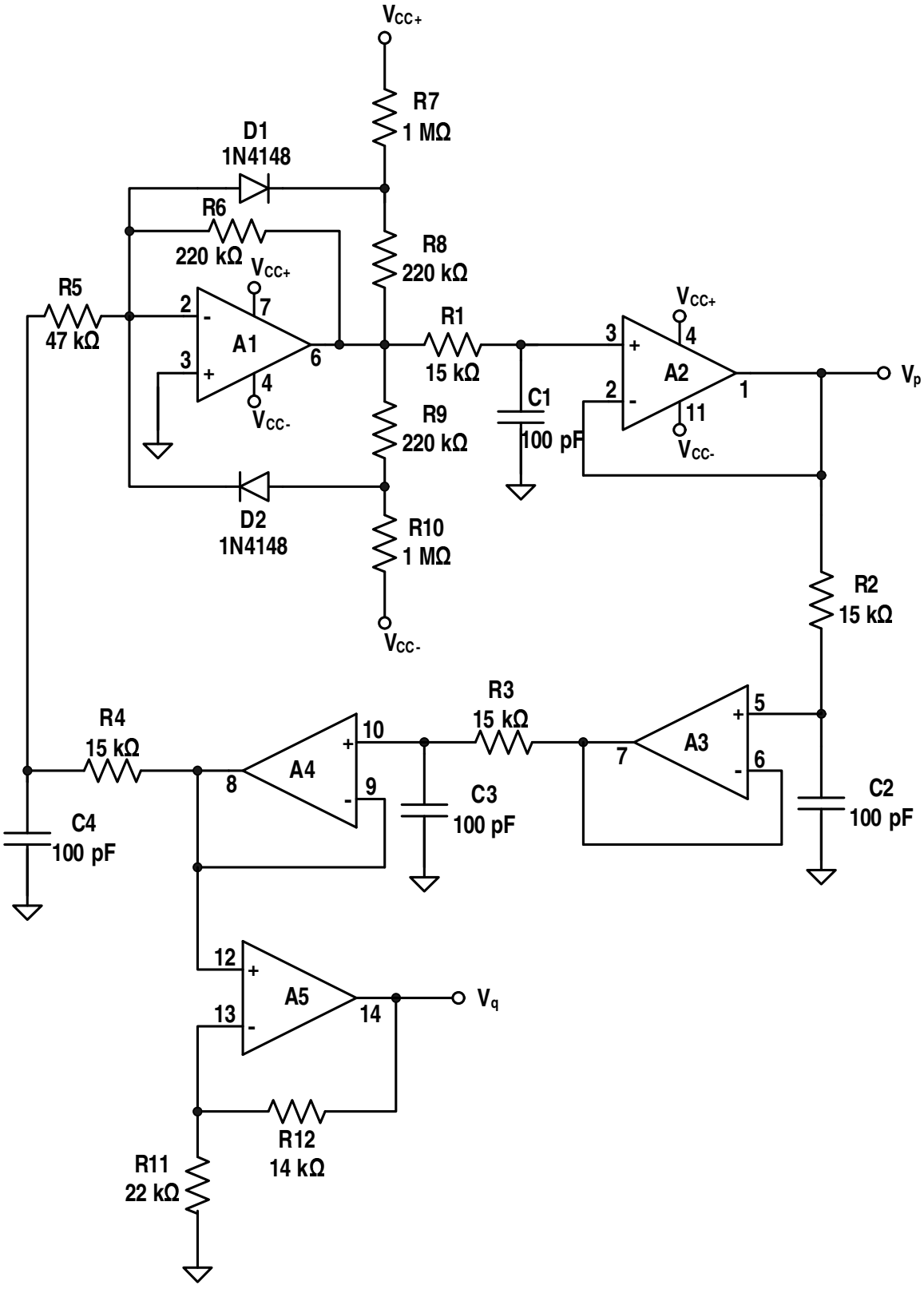

Fig. 4.3 Circuit diagram of Bubba oscillator (A1: LF356, A2 – A5: TL084).

Table 4.1 Comparison of amplitude stability of the Wein bridge oscillator circuits of Fig. 4.1 and 4.2, the Bubba oscillator of Fig. 4.3, and HP33120A.

Signal source	Amplitude variation	Average V_{pp} (V)	ΔV_{pp} (V)	% Variation
Wein bridge oscillator of Fig. 4.1	+4.13 V: +4.26V -4.24 V : -4.31 V	8.47	0.2	2.36
Wein bridge oscillator of Fig. 4.2	+7.64 V : +7.72 V -7.56 V : -7.61 V	15.265	0.13	0.85
Bubba oscillator of Fig. 4.3	+3.458 V : +3.476 V -3.372 V : -3.348 V	6.827	0.042	0.62
HP33120A	+3.408 V : +3.434 V -3.308 V : -3.290 V	6.72	0.044	0.65

The actual phases at the various stages of the circuit were measured. The phase difference between V_p and

(i) $V_q = 85^\circ$

(ii) waveform at output of A3 = 41.33°

(iii) waveform at output of A4 = 81.5°

To avoid loading due to R_4-C_4, a non-inverting buffer was inserted after it and the actual phases at the various stages of the circuit were measured. The phase difference between V_p and

(i) $V_q = 83.5^\circ$

(ii) waveform at output of A3 = 40.9°

(iii) waveform at output of A4 = 82.9°

4.3 Demodulator section

The demodulator section in the existing instrument is shown in Fig. 4.4. It consists of a precision rectifier and a low pass filter to get the envelope of the amplitude modulated waveform. But at 100 kHz, because of phase shifts, the amplitudes of the positive and negative half cycles do not properly align, this results in a nonlinear relationship between the input amplitude and rectified output. Using opamp CA3100,

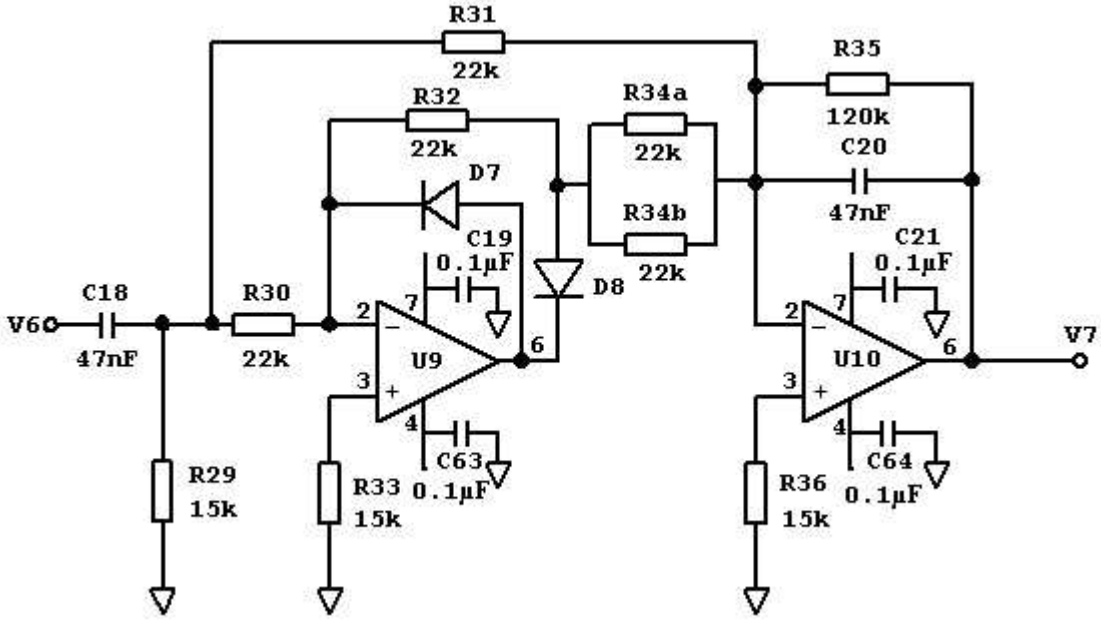

Fig. 4.4 Fullwave precision rectifier based demodulator circuit in the existing instrument [20] (U9, U10: LF356).

with gain-bandwidth product of 38 MHz did not solve the problem. It was decided to use a synchronous detector, using a fast analog multiplier. Use of synchronous detector will permit better noise rejection and simultaneous multifrequency measurements. Further, in order to facilitate measurement of complex impedance, it was decided to use vector lock-in amplifier, which will give in-phase and out-of phase components of the envelope.

4.3.1 Vector lock-in technique

A vector lock-in amplifier involves synchronous detection of the amplitude modulated signal with two references, the carrier itself and its 90° phase shifted version. The basic block diagram of vector lock-in amplifier [30] is given in Fig. 4.5. Here the input to the system under test is the carrier signal, V_p. The output obtained from S.U.T. is an amplitude modulated waveform. This is then multiplied with the same carrier that was used for modulation and the output obtained is passed through a low pass filter whose cut-off is such that only the modulating signal can pass through. The output obtained, p will be the in-phase component of the modulating signal with respect to the carrier. A 90° phase shifted version of the carrier, V_q, is multiplied with the modulated waveform and low pass filtered. This gives the quadrature component, q. A vector calculator then calculates the magnitude and phase of the modulating signal using Eqn. 4.3 and 4.4.

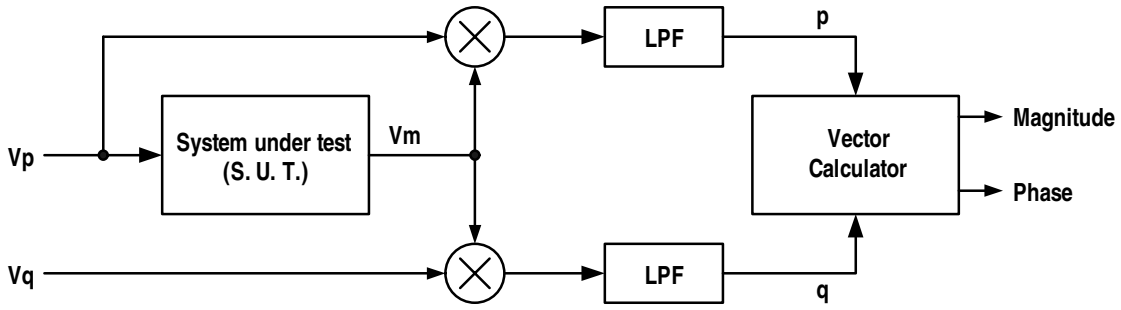

Fig. 4.5 Block diagram of vector lock-in technique.

$$Magnitude = \sqrt{p^2 + q^2} \tag{4.3}$$

$$Phase = \tan^{-1}\left(q / p\right) \tag{4.4}$$

4.3.2 Circuit used for vector lock-in technique

The vector lock-in amplifier was realized by using fast analog multiplier AD633, as shown in Fig. 4.6. The modulated waveform obtained at the output of the instrumentation amplifier of the ICG extraction circuit, V_m, is fed as inputs to both the multipliers. The two phase shifted oscillator outputs, V_p and V_q, are applied as the other multiplying input. The outputs obtained at pin number 7 is then low pass filtered by R_1, C_1, R_2 and C_2 to get the in-phase, p, and out-of-phase, q, components of the modulating signal.

4.3.3 Test results

This technique was tested by modulating a known signal with a known carrier signal and then demodulating it to obtain the modulating signal. The modulating signal used was a 1 Hz sine wave and the carrier signal used was the 100 kHz sine wave from the Bubba oscillator. The output of the in-phase component was found to be around 15 times the quadrature component, *i.e.*, the in-phase output to quadrature output ratio is 23.5 dB. The quadrature component was present because the phase difference between the two oscillator outputs was observed to be 88°.

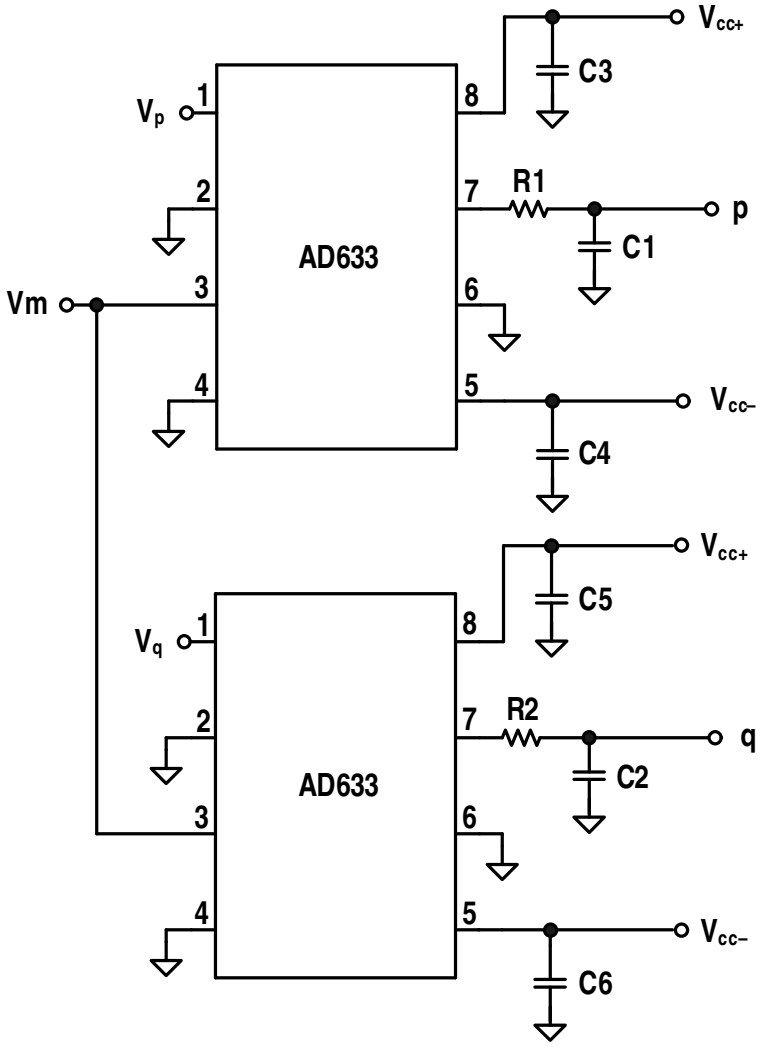

Fig. 4.6 Circuit diagram of lock-in technique.

4.4 Baseline restoration circuit

In the varying impedance signal, the amplitude of the varying portion is typically only 1 to 2% of the basal impedance. Thus if the signal is used as such, only a portion of the available range of ADC can be used for analysis of the signal. Therefore it is required that the DC part be removed and only the AC part be used for further processing. But the basal impedance of different subjects is different, and there are various artifacts.

4.4.1 Block diagram

For this problem, a microcontroller based baseline restoration circuit was

developed earlier [20][31] whose block diagram is shown in Fig. 4.7. Whenever the output voltage crosses the range set by two pre-defined thresholds, it is detected by comparison and the microcontroller then varies the duty cycle of its PWM (pulse width modulation) output accordingly so that constant DC voltages are subtracted or added to the input in steps until the signal is brought within the threshold range. Even if the basal impedance drifts, this circuit accordingly changes the DC voltage subtracted or added. The existing circuit has an output range of [-2.5, -1] V. This needs to be changed to [-4, 4] V because the input range of the ADC is ±5 V. DC parts in both the positive as well as negative sides can be removed now with the program modified to start with 50%

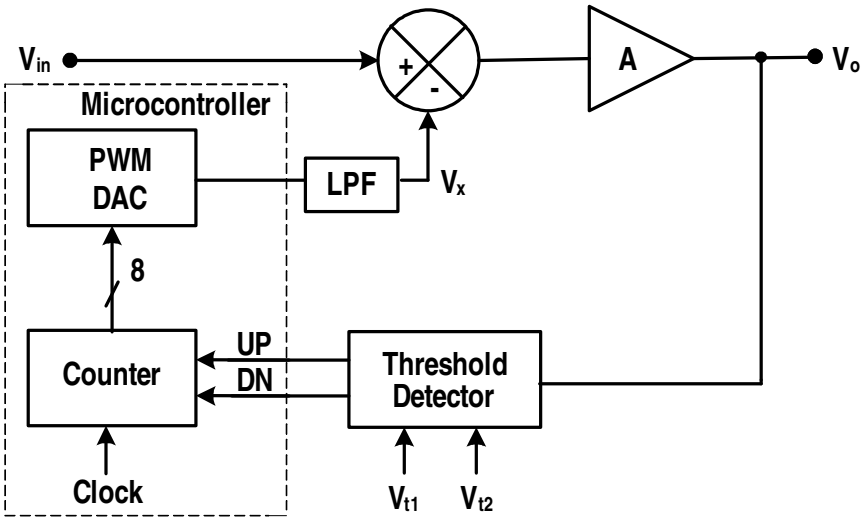

Fig. 4.7 Block diagram of baseline restoration circuit.

duty cycle which corresponds to no DC offset. The amplifier configuration was changed from inverting to non-inverting. This work was jointly done along with Mr. Vinod Kumar Pandey [32].

4.4.2 Circuit Diagram

The circuit diagram is given in Fig. 4.8. Threshold voltages, V_{t1} and V_{t2}, are obtained by using a resistive voltage divider. The output voltage is compared with the thresholds using comparators, U1B and U1C, and the outputs of the comparators are connected to port pins P1.0 and P1.1 of the microcontroller. The tracking up/down counter is realized using software inside the microcontroller. The count value is output as

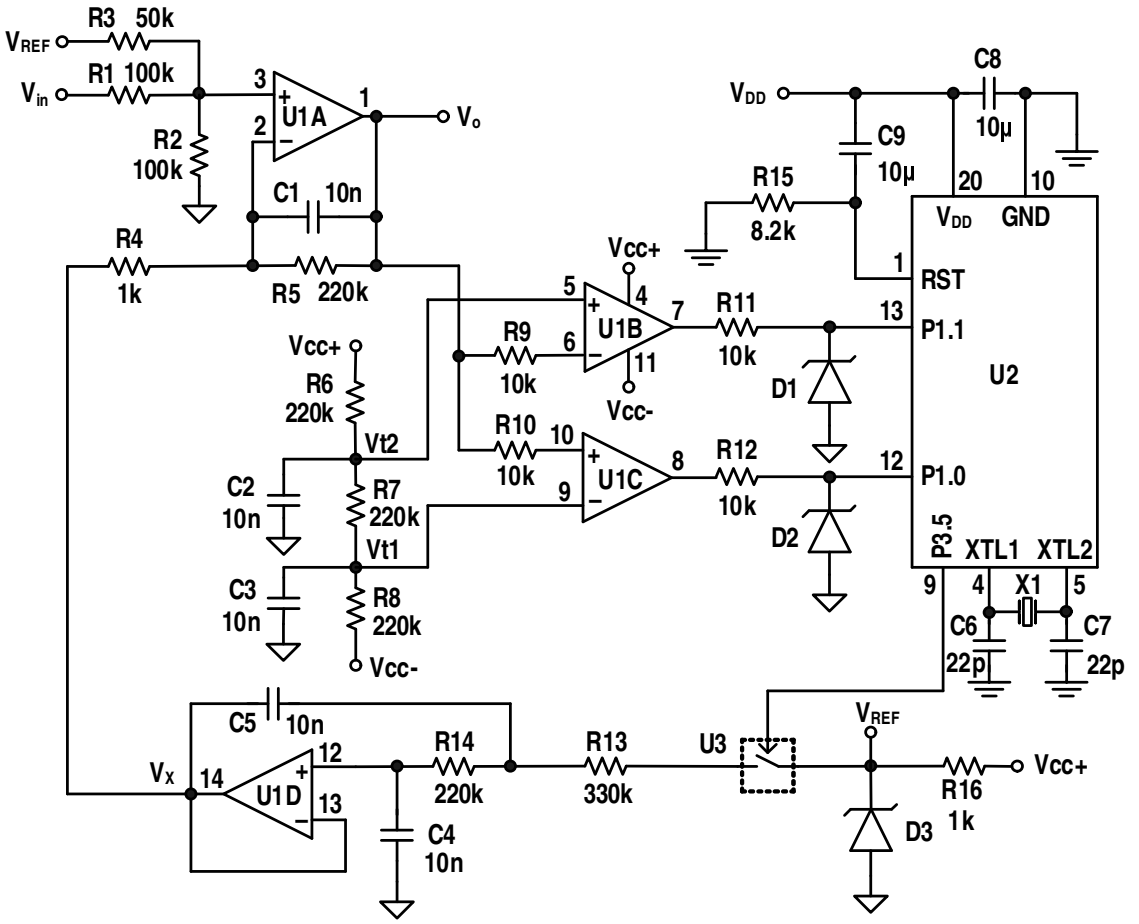

Fig. 4.8 Circuit diagram of baseline restoration circuit (U1: TL084, U2: AT89C2051, U3: CD4066, D1 = D2 = D3 = 4.7 V Zener).

PWM as an approximation to the baseline drift. The PWM pulses are low pass filtered by second order low pass filter formed by U1D with a cut off frequency of 60 Hz. The PWM is implemented in software with a clock frequency of 7.8 kHz. A voltage reference, D3, has been used to stabilize the amplitude of the PWM. Whenever the signal after amplification crosses the threshold range, the duty cycle of the PWM output is correspondingly changed such that the output signal is brought to the middle of the threshold range.

This circuit was tested by providing an input of 15 mV (p-p) sine wave of 20 Hz superimposed on a dc offset of + 2 V with a triangular drift of 60 mV (p-p) and 0.5 Hz. Output signal shows that the baseline has been restored and the drift is compensated when the signal crosses the threshold range as shown in Fig. 4.9.

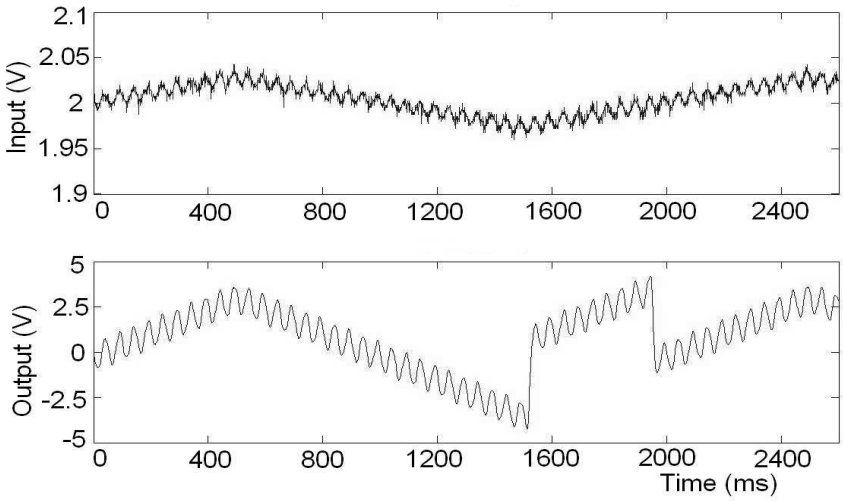

Fig. 4.9 Example of baseline restoration.

Chapter 5
THORACIC IMPEDANCE SIMULATOR

5.1 Introduction

A thoracic impedance simulator is necessary for testing and calibration of the impedance cardiograph instrument and has been developed based on earlier designs [19][20][33]. It generates step changes in impedance simulating the change in impedance with each cardiac cycle which can be used for finding the sensitivity and response time (or bandwidth) of the impedance cardiograph. It also generates square waves of known magnitude to simulate the ECG sensed by the impedance cardiograph both in differential mode as well as common mode for testing the gain and CMRR of the ECG instrumentation amplifier. The unit can provide signals for testing/calibration of (a) the ICG extraction circuit, or (b) the ECG extraction circuit. It can work in only one of these modes at a time. Option for feeding external pick-ups is also incorporated. The simulator is powered by a 9 V battery. The earlier design used astable multivibrators, manual switches and potentiometers. This has been replaced by a microcontroller based circuit which takes inputs from two soft keys and has a LCD for display and selection of various options.

5.2 Thoracic impedance simulator model

The impedance model of the thorax, used in the simulator is shown in Fig. 5.1. The high frequency current is injected through the inputs I1 and I2. The variation in impedance is sensed through the outputs E1 and E2. In this model, R_e's constitute the tissue-electrode contact resistances for 4-electrode configuration. Resistances R_o and R_s are the parallel column model resistances and R_{s1} and R_{s2} are the fixed resistances in the current path. Option for feeding external pick-up is denoted by V_p and the resistance in the pick-up path by $R_{p.}$ The external ground refers to the ground of the impedance

cardiograph instrument while the internal common refers to the ground of the thoracic impedance simulator. The voltage sources V_{ed} and V_{ec} represent the differential mode and common mode ECG signals respectively. A very simplified simulation of the variation in the thoracic impedance is used here. The net resistance, switches between R_o and $R_s \parallel R_o$ in response to cardiac systole pulses. This pulsating change in the resistance is useful for calibration of the impedance detector unit.

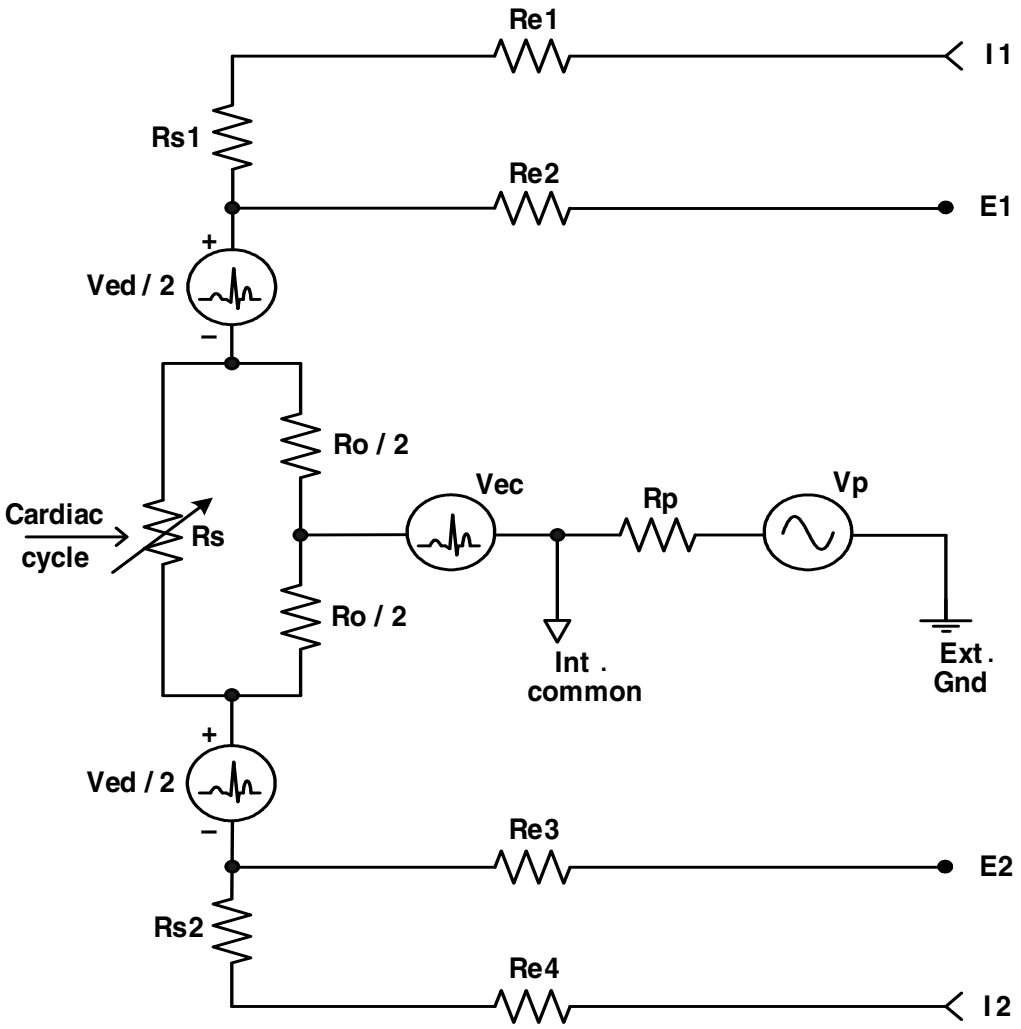

Fig. 5.1 Thoracic impedance model.

5.3 Model relations with the schematic

The thorax model of Fig. 5.1 has several sources without a common node. These are difficult to realize in an electronic circuit without using transformers. In order to have an easily realizable circuit, the model can be modified to a schematic shown in Fig. 5.2.

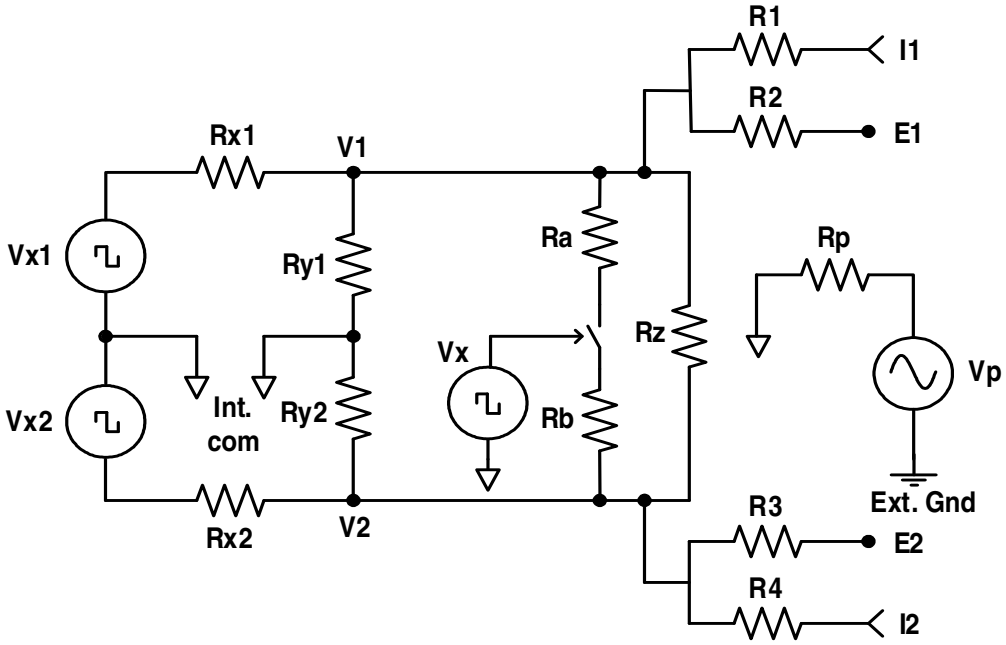

Fig. 5.2 Schematic of the model shown in Fig. 5.1.

Relations of the component values in the schematic of Fig. 5.2 to those in the model of Fig. 5.1 are as the following

$$R_1 = R_{s1} + R_{e1} \tag{5.1}$$

$$R_2 = R_{e2} \tag{5.2}$$

$$R_4 = R_{e4} + R_{s2} \tag{5.3}$$

$$R_3 = R_{e3} \tag{5.4}$$

$$R_a = R_b = \frac{R_s}{2} \tag{5.5}$$

$$R_z = R_o \tag{5.6}$$

Let us represent the common mode and differential mode ECG voltages in Fig. 5.1 by

$$V_1 = V_{ec} + \frac{V_{ed}}{2} \tag{5.7}$$

$$V_2 = V_{ec} - \frac{V_{ed}}{2} \tag{5.8}$$

In Fig. 5.2, we have

$$V_1 = V_{x1}\left[\frac{R_{y1}'}{R_{x1} + R_{y1}'}\right] \tag{5.9}$$

$$V_2 = V_{x2}\left[\frac{R_{y2}'}{R_{x2} + R_{y2}'}\right] = V_{ec} - \frac{V_{ed}}{2} \tag{5.10}$$

where,

$$R_{y1}' = R_{y1} \parallel \left(R_z + \left(R_{y2} \parallel R_{x2}\right)\right),\ R_{y2}' = R_{y2} \parallel \left(R_z + \left(R_{y1} \parallel R_{x1}\right)\right)$$

5.4 Hardware blocks of the simulator

The circuit development for the schematic of Fig. 5.2 is shown in Fig. 5.3 and is described below. The impedance switching is realized using quad analog switches in IC 4066. The heart beat and CM/DM ECG generation is done using a microcontroller. There is a small circuit for obtaining Vcc+ and Vcc– from a single supply.

Thorax impedance simulator

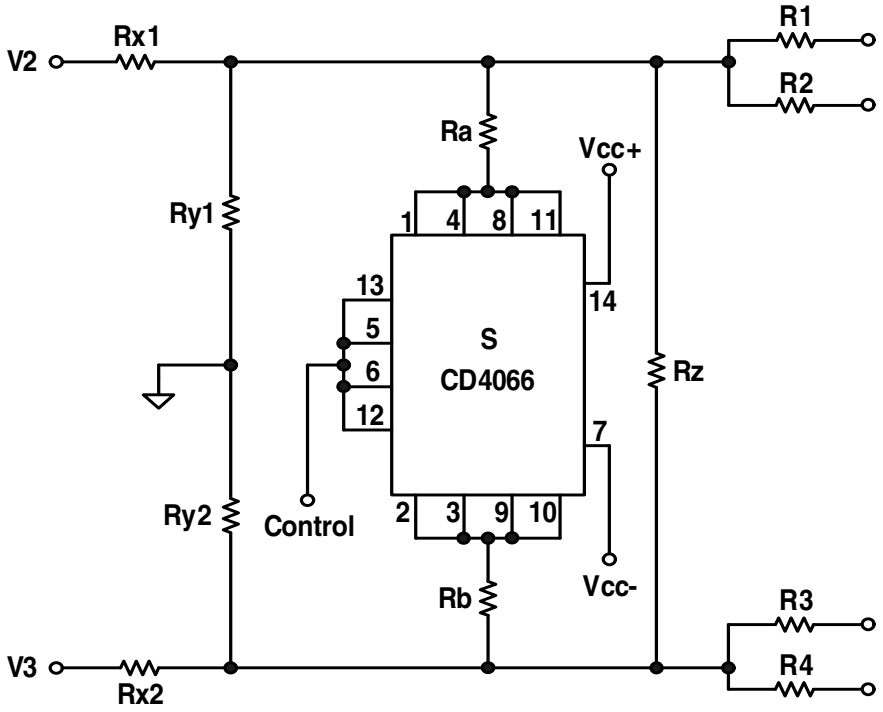

Fig. 5.3 Circuit diagram of thoracic impedance simulator.

The circuit diagram of the thorax impedance simulator is shown in Fig. 5.3. The 4 analog switches in IC CD4066 are paralleled together for a reduced “on” resistance.

$$R_{eq(on)} = R_z \parallel (R_a + R_b + R_{s(on)}) \parallel ((R_{x1} \parallel R_{y1}) + (R_{x2} \parallel R_{y2})) \tag{4.11}$$

$$R_{eq(off)} = R_z \parallel (R_{y1} + R_{y2}) \parallel (R_a + R_b + R_{s(off)}) \quad (4.12)$$

CD4066 analog switches have typical on-resistance of 270 Ω (for $V_{DD} - V_{SS} \approx 5$ V). In the circuit used, two values of basal impedances are simulated as shown in Fig 5.4. The first value is obtained when $R_z = R_{34}$. In this case, there are two values of change in impedance, which can be selected corresponding to branch R_{s8} or R_{s9} being switched where R_{s8} and R_{s9} represent the resistance of analog switches U8 and U9 respectively.. The second value is obtained when $R_z = R_{34} \parallel (R_{32} + R_{s9(on)} + R_{33})$. In this case, there is only one value for change in impedance corresponding to branch R_{s8} being switched.

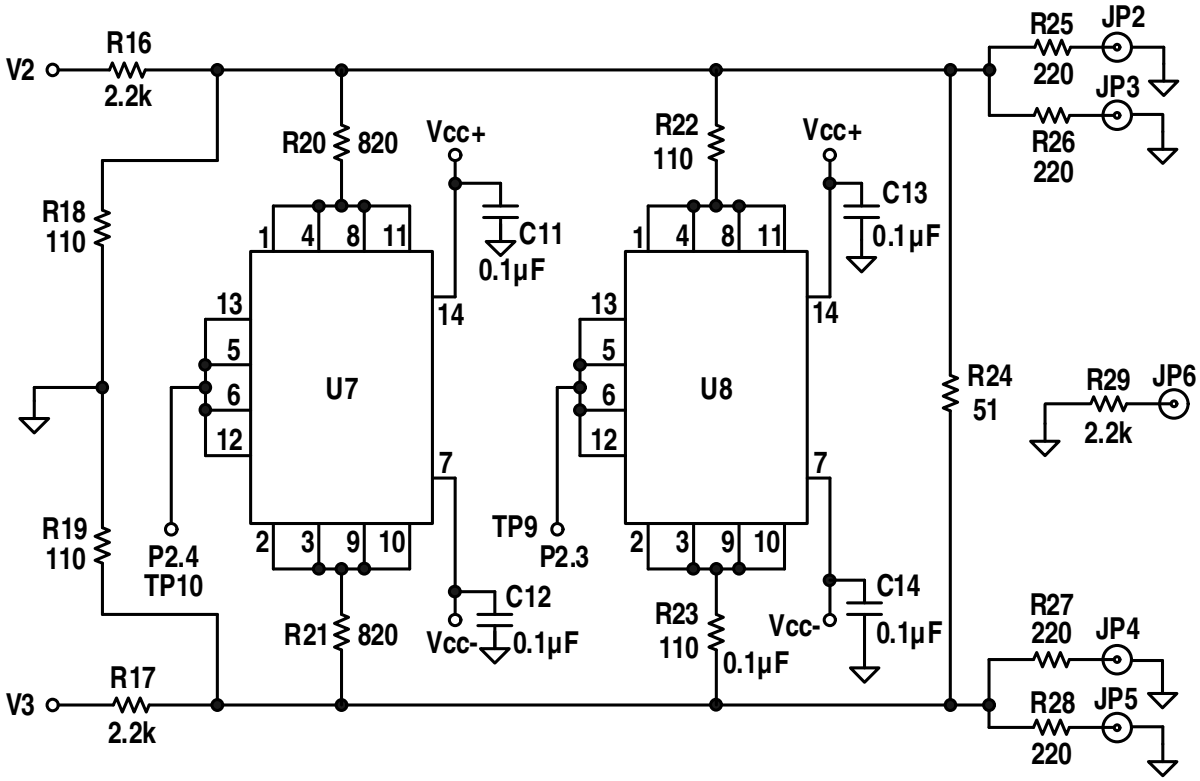

Fig. 5.4 Circuit diagram of multi-basal thoracic impedance simulator used (U8, U9: CD4066).

Power supply

The power supply circuit generates +5 V and ground for the digital section and +2.5 V, -2.5 V and ground for the analog section as shown in Fig. 5.5. It consists of two voltage regulators, U1 and U2, which give +5 V at their output. The output of U2 is given to an opamp (U3A) based split power supply to give +2.5 V and –2.5 V with respect to the analog ground.

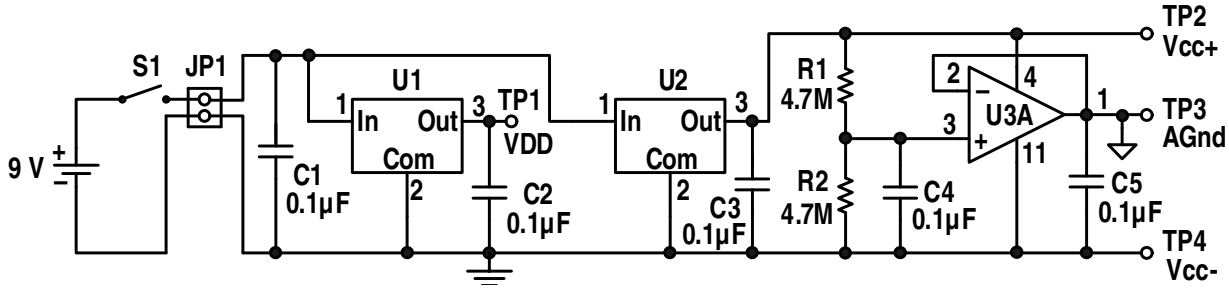

Fig. 5.5 Circuit diagram of power supply (U1, U2: LM7805, U3: LM324).

CM / DM ECG generator

A reference voltage of 1.25 V is generated using a voltage reference IC, U4. This voltage is then given to an amplitude control circuit built around U3B as shown in Fig 5.6. Depending on the switch combinations, the amplitude can be scaled to 0X, 0.1X, 0.2X and 1.0X as given in Table 5.1. The output voltage, V1, is given to two polarity controlled amplifiers which are controlled by switches such that the output switches between +V1 and –V1 for each polarity controlled amplifier. The control signals for the switches are generated by the microcontroller in such a way that V2 and V3 are square waves either in-phase for common mode or out-of-phase for differential mode. The polarity controlled amplifiers are formed around U3C and U3D.

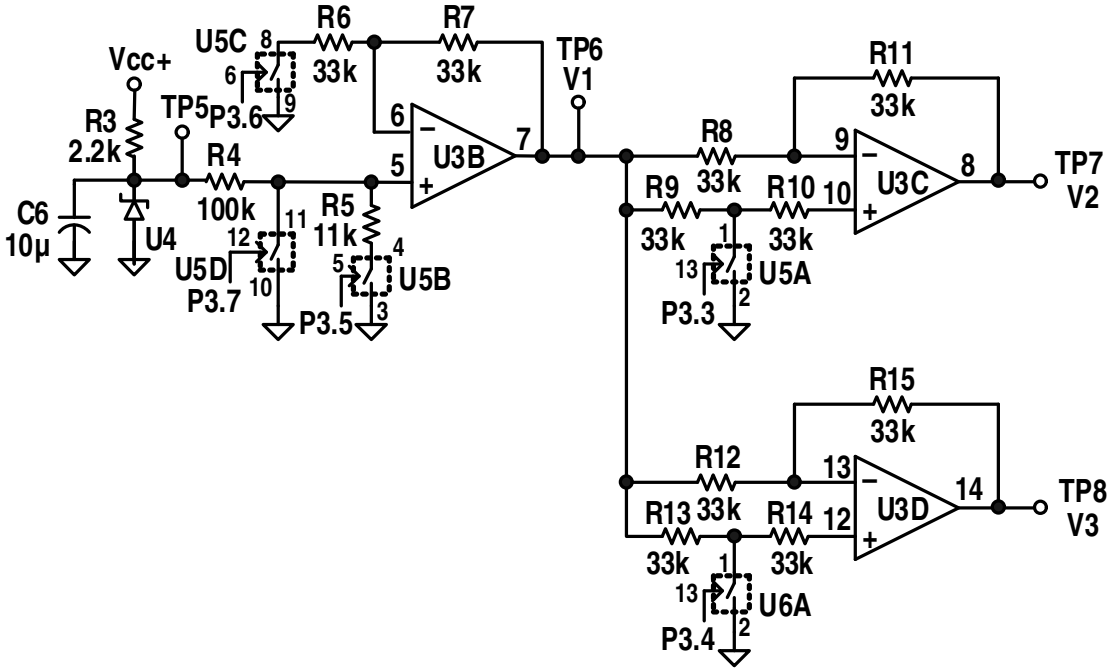

Fig. 5.6 Circuit diagram of ECG amplitude control (U4: LM385-1.2, U5, U6: CD4066).

Table 5.1 Switch configurations for ECG amplitude control.

U5D	U5B	U5C	V1
On	X	X	0X
Off	On	Off	0.1X
Off	On	On	0.2X
Off	Off	Off	1.0X

5.5 Digital control of the operation

A 40-pin microcontroller AT89C52 has been used for user control of the simulator circuit, with the objective of reducing long signal tracks and wires. Two keys and a 16 character-by-two line LCD are used for user interface. The pin assignment is given in Table 5.2 and is also shown in Fig. 5.7.

Basically there are two modes of operation, *i.e.*, ICG and ECG. In ICG, there are options for changing the frequency, f, basal impedance, Z_o, and percentage change in impedance, Δz, using the soft keys. Within ECG, there are two modes- common mode (C) and differential mode (D). In each of these modes, the frequency and the amplitude can be varied. The LCD shows the current mode and the value of the variable parameters. There are two soft keys, *i.e.*, Function and Change. The Function key selects the various options one-by-one in a cyclic manner. The parameter which is currently selected is shown blinking. The Change key allows the user to vary the parameters through a set of

Table 5.2 Assignment of pins for various functions on the microcontroller.

Port pin	Function
P1.0 – P1.7	LCD Data pins
P3.0	Enable of LCD
P3.1	RW of LCD
P3.2	RS of LCD
P3.3, P3.4	ECG square wave generation
P3.5, P3.6, P3.7	ECG amplitude control
P2.0, P2.1	Soft keys
P2.4, P2.5	ICG control signals

different choices available for it in a cyclic manner. The mode/parameter options are as shown in Fig. 5.8. The percentage change in impedance was designed for 10 % and 2 % but due to the standard values of resistors available, it deviated from the desired values.

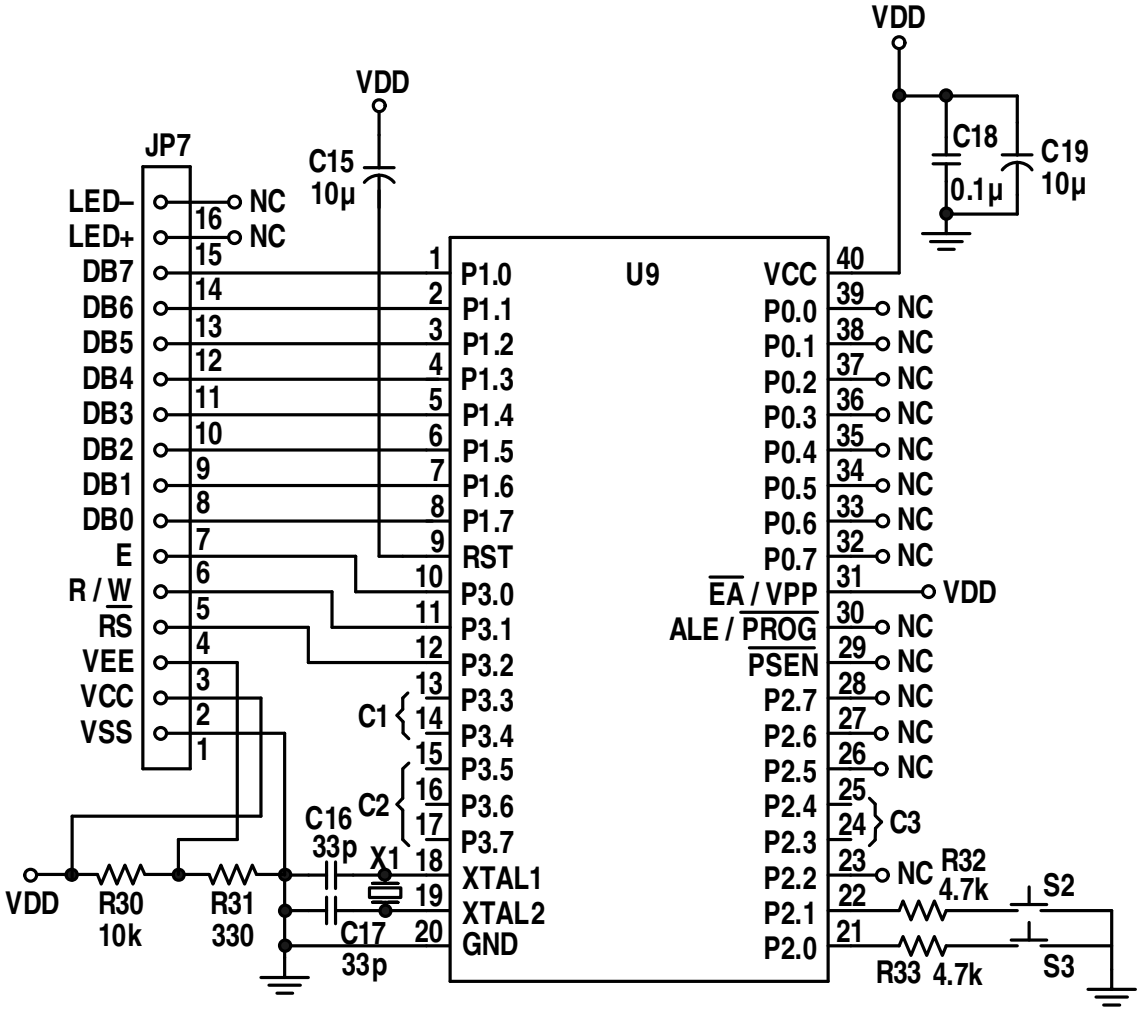

Fig. 5.7 Circuit diagram showing the microcontroller for controlling the thoracic impedance simulator (C1: ECG square waves, C2: control signals for ECG amplitude control, C3: ICG switching control signals, U9:AT89C52, JP7:LCD).

5.6 Software

The software has to take care of interfacing the two soft keys and LCD display. It also has to generate square waves for ECG, control signals for ECG amplitude control and square waves for ICG control signal. The algorithm used is as follows:

1. Start.
2. Generate control signals and square waves in default mode and display.
3. Check for key press.

4. If first key is pressed,

   Select the next parameter, goto 3.

5. If second key is pressed,

   if no parameter is active, goto 3

   if any parameter is active,

   Change the currently active parameter to its next value, goto 3.

6. Generate control signals and square waves as per the current settings.

7. Display current settings for the user.

8. Goto 3.

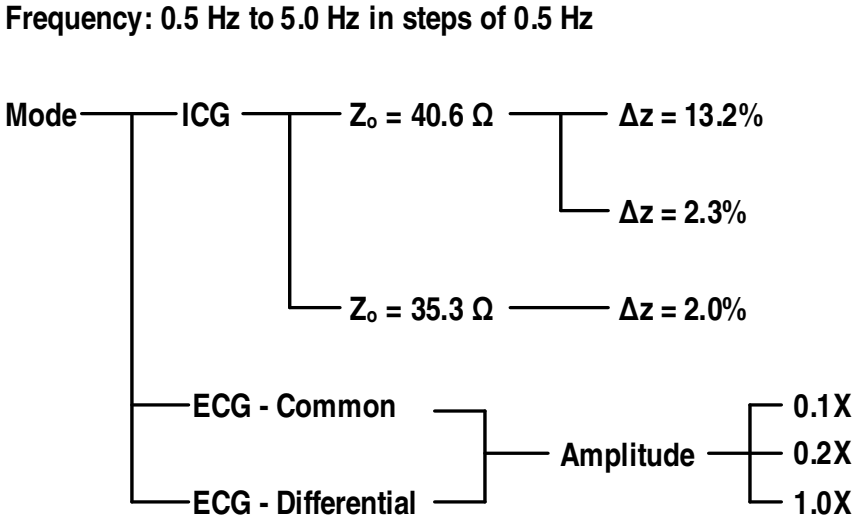

Fig. 5.8 Mode/parameter options in the thoracic impedance simulator.

5.7 PCB Design and assembly

A PCB for the simulator was designed, with proper decoupling of all the IC's and a ground plane has been formed on the top (component) side of the board. The assembled board has been boxed. It has been tested and has been found to be working satisfactorily.

5.8 Test results

The different modules of the thoracic impedance simulator have been validated and the test results are presented in this section.

5.8.1 ECG amplitude control

The reference voltage, V_{ref}, was measured to be 1.253 V. The output voltages obtained at the different scaling factors is given in Table 5.3. This voltage was obtained by finding the peak-to-peak amplitude of the square wave at TP7 in Fig 5.6.

Table 5.3 ECG square wave amplitude at TP7.

Scaling factor	Peak-to-peak voltage at TP7
0.1X	120 mV
0.2X	245 mV
1.0X	1.23 V

5.8.2 ICG impedance switching

The actual impedance values were measured using a multimeter (HP 34401A) across R24 in Fig 5.4 and are tabulated in Table 5.4.

Table 5.4 Actual levels of impedance as measured by multimeter (HP 34401A).

Nominal Z_o (Ω)	Measured Z_o (Ω)	Nominal Δz (%)	Measured Δz (%)
40.6	41.15	13.2	10.3
		2.3	2.4
35.3	35.8	2.0	2.0

5.8.3 Frequency

The frequency of the output ECG square waves and impedance switching was measured with a frequency counter and actual values were within 1% of the nominal value.

5.8.4 Testing with the existing instrument and modified circuit

The built simulator was connected to the impedance cardiograph instrument developed by Manigandan [20] and the $-z(t)$ waveform from the impedance cardiograph was recorded and shown in Fig. 5.9 and 5.10. The simulator was also connected with the impedance cardiograph circuit modified during the course of this project and the $-z(t)$ waveform obtained was recorded and shown in Fig. 5.11.

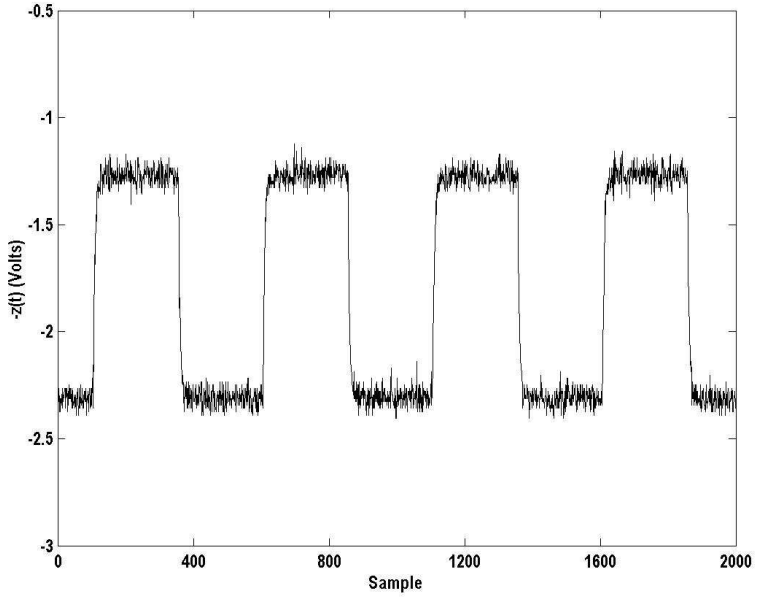

Fig. 5.9 Output $-z(t)$ obtained from Manigandan's impedance cardiograph instrument [20] when connected to the developed thoracic impedance simulator (Z_o = 35.3 Ω, Δz = 2.0 %).

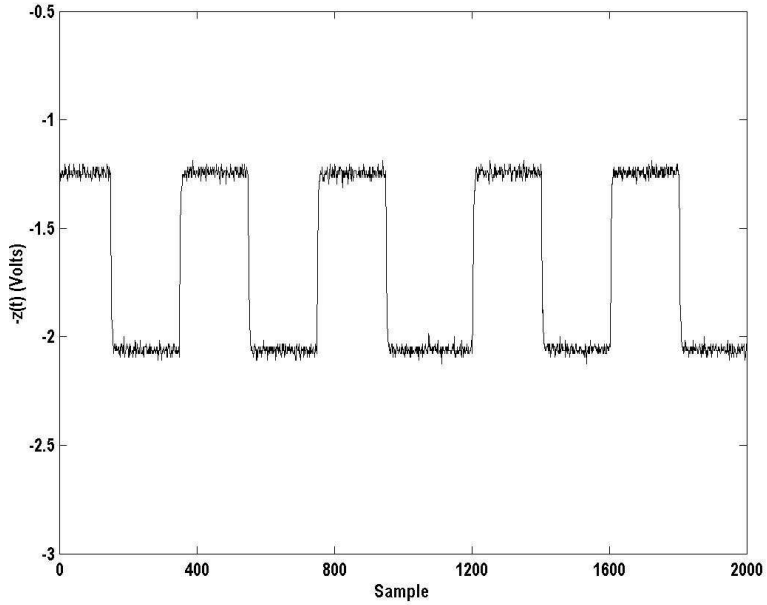

Fig. 5.10 Output $-z(t)$ obtained from Manigandan's impedance cardiograph instrument [20] when connected to the developed thoracic impedance simulator (Z_o = 40.6 Ω, Δz = 2.3 %).

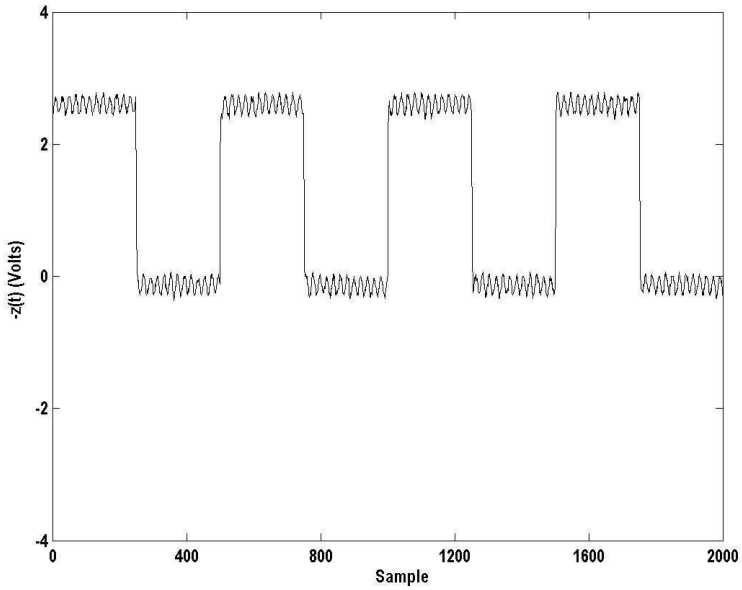

Fig. 5.11 Output $-z(t)$ obtained from the modified circuit when connected to the developed thoracic impedance simulator (Z_O = 40.6 Ω, Δz = 13.2 %).

The output of the instrumentation amplifier of the impedance cardiograph instrument developed by Manigandan [20] was recorded with the developed simulator in ECG differential mode and shown in Fig. 5.12.

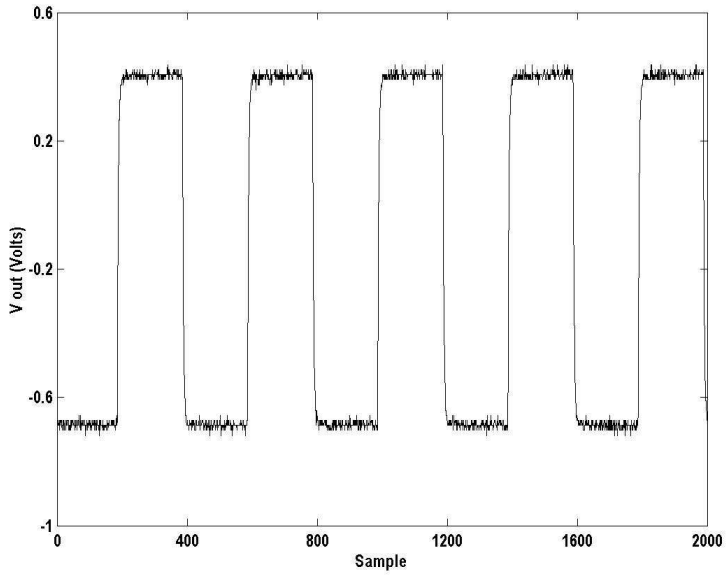

Fig. 5.12 Output of instrumentation amplifier when differential mode ECG signal is given as input from the developed simulator (Amplitude scaling factor: 1.0X).

Chapter 6
SUMMARY AND CONCLUSIONS

6.1 Summary of work done

The project objective was to improve the hardware for impedance cardiography, making use of the previous designs, and making appropriate modifications. A literature review was carried out and the existing instrument was studied. The Wein bridge oscillator was modified to improve its short term amplitude stability. A study on different oscillators was carried out in terms of short term amplitude stability and a quadrature oscillator called Bubba oscillator was chosen due to its amplitude stability and low distortion. Vector lock-in amplifier has been chosen in place of the precision rectifier based demodulator. The parameters of the baseline restoration circuit have been modified for better performance. The existing thoracic impedance simulator was upgraded by using a microcontroller based circuit and providing LCD and soft keys for user interaction. The simulator has been assembled and boxed.

6.2 Suggestions for future work

A DC battery powered power supply has to be designed to make it portable and safe for clinical recordings. Powerline interference is one of the problems right now. So after designing the power supply, the PCB for the instrument can be made. Using synchronous detector technique, multi-frequency impedance measurement scheme can be implemented and respiration related impedance signal can be obtained from a different site and used for removal of respiration artifact from the ICG signal. The impedance simulator can be further improved by using digital potentiometers to give a wide range of choice for basal impedance and change in impedance for the user.

Appendix A
SOME IMPEDANCE CARDIOGRAPH INSTRUMENTS

A.1 Minnesota impedance cardiograph

This was developed at the University of Minnesota by Kubicek *et al.* [7] and was the first available instrument (1974). Four aluminium-coated Mylar electrode strips, two around the neck and two around the abdomen are used. The injected current is a sinusoidal alternating current of 2 mA rms at 100 kHz. The stroke volume is calculated using Eqn. 2.7. It is available through Bio-Impedance Technology Inc. (Chapel Hill, NC, USA) as models HIC-2000 and HIC-3000 (HIC – Hutcheson impedance cardiograph) [37].

A.2 BioZ

CardioDynamics International Corporation (CDIC) (San Diego, Cal., USA) [10], manufactures impedance cardiograph instrument with the name BioZ and has GE Healthcare and Philips Medical Systems as its partners. The injected current is a maximum of 4 mA rms at a minimum frequency of 60 kHz. The electrode configuration used is the same as that used by Sramek [8]. A proprietary modification to the Sramek-Bernstein equation (ZMARC – impedance modulating aortic compliance) is used for the calculation of stroke volume [34].

A.3 NICOMON

Larsen and Toubro (L&T) Medical Equipment and Systems (Mysore, India) [11] has brought out an impedance cardiograph instrument having the name NICOMON (non-invasive cardiac output monitor) with technology transfer from Bhabha Atomic Research Centre (BARC, Mumbai, India). This is the result of research by Jindal *et al.* [35][36]. The electrode configuration used is the same as that used by Sramek [8]. The injected current has a frequency of 50 kHz and the amplitude can be selected to be either 2 mA or 4 mA. The stroke volume is calculated using Eqn. 2.7.

A.4 Mindware ambulatory impedance cardiograph

Mindware Technologies (Gahanna, Ohio, USA) manufactures an ambulatory impedance cardiograph that is small enough to be worn on a belt (MW1000A) [12]. It uses an injection current of 400 μA at 100 kHz. They also have a desktop version (MW2000D).

A.5 Physio flow

Manatec Biomedical (Paris, France) manufactures impedance cardiograph instrument named Physio Flow. It uses six pre-gelled Ag-AgCl electrodes on the thorax [13] with two electrodes for sensing the ECG. The injection current used is of 3.8 mA (peak-to-peak) at 75 kHz. They claim to have avoided the use of Z_o in the calculation of cardiac output.

A.6 IQ

Wantagh Inc. (Bristol, UK) manufactures impedance cardiograph instrument named IQ [14][38]. It uses an injection current of 4 mA at 100 kHz. The stroke volume is calculated using time, frequency and power analysis of the ICG signal. The electrode configuration used is the same as that used by Sramek [8] plus three electrodes are used separately for ECG.

A.7 HOTMAN system

Hemo Sapiens Inc. (AZ, USA) manufactures a system named HOTMAN (hemodynamic and oxygen transport management) as well as a module named TEBCO (thoracic electrical bioimpedance cardiac output) [15]. This is a result of research by Sramek [8].

Appendix B

LIST OF COMPONENTS

Thoracic impedance simulator

Component designator	Part description	Component specification	Approx. price/unit in Rs.
R1, R2	Resistor	4.7 MΩ, 1/4 Watt	0.50
R3, R16, R17, R29	Resistor	2.2 kΩ, 1/4 Watt	0.50
R4	Resistor	100 kΩ, 1/4 Watt	0.50
R5	Resistor	11 kΩ, 1/4 Watt	0.50
R6 – R15	Resistor	33 kΩ, 1/4 Watt	0.50
R18, R19, R22, R23	Resistor	110 Ω, 1/4 Watt	0.50
R20, R21	Resistor	820 Ω, 1/4 Watt	0.50
R24	Resistor	51 Ω, 1/4 Watt	0.50
R25 – R28	Resistor	220 Ω, 1/4 Watt	0.50
R30	Resistor	10 kΩ, 1/4 Watt	0.50
R31	Resistor	330 Ω, 1/4 Watt	0.50
R32, R33	Resistor	4.7 kΩ, 1/4 Watt	0.50
C1 – C5, C7 – C14, C18	Ceramic capacitor	0.1 µF	0.40
C6, C15, C19	Electrolytic capacitor	10 µF	1.00
C16, C17	Ceramic capacitor	33 Pf	0.40
S1	Switch	SPDT	8.00
S2, S3	Soft keys		10.00
U1, U2	IC	LM7805	10.00
U3	IC	LM324	10.00
U4	Voltage reference	LM385-1.2	10.00
U5, U6, U7, U8	IC	CD4066	9.00
U9	IC	AT89C52	200.00
Battery		9 V	40.00
JP1	2-pin male connector		1.50
JP2 – JP6	RCA connector		5.00
JP7	16 character by two line LCD		150.00
TP1 – TP10	Test pins		0.50
		Total cost	555.00

Note: All resistors are of 1% tolerance.

Appendix C

MICROCONTROLLER PROGRAMMING

Values stored in the EEPROM

Location 0x0800 to 0x0809:
Look-up table storing the count values for generating the different frequencies.

Location 0x0900 to 0x09FF:
Look-up table storing values 00H to 0FFH in bit reversed order for reversing the port pins for the data bits of the LCD.

Functions of the various registers

Register	**Function**	**Value**	
R0	Current count value for frequency	-	
R1	Key pressed	01 - Second key 10 - First key	
R2	Current mode	00 – ICG 01 - ECGC 02 – ECGD	
R3	Current ECG amplitude	00 - 0.1X 01 - 0.2X 02 - 1.0X	
R4	Active parameter	ICG 00 - no parameter 01 - Mode 02 - Frequency 03 - Basal impedance Z_o 04 - Change in impedance Δz	ECG 00 - no parameter 01 - Mode 02 - Frequency 03 - Amplitude

R5	Current ICG basal impedance selection	00 - 40.6 Ω 01 - 35.3 Ω
R6	Current ICG change in impedance selection	00 - 13.2 % 01 - 2.3 % 02 - 2.0 %
R7	Currently selected frequency option	00 to 09 with 00 corresponding to 0.5 Hz and 09 to 5 Hz with the in-between values in increments of 0.5 Hz.

Appendix D

PCB LAYOUT

Thoracic impedance simulator:

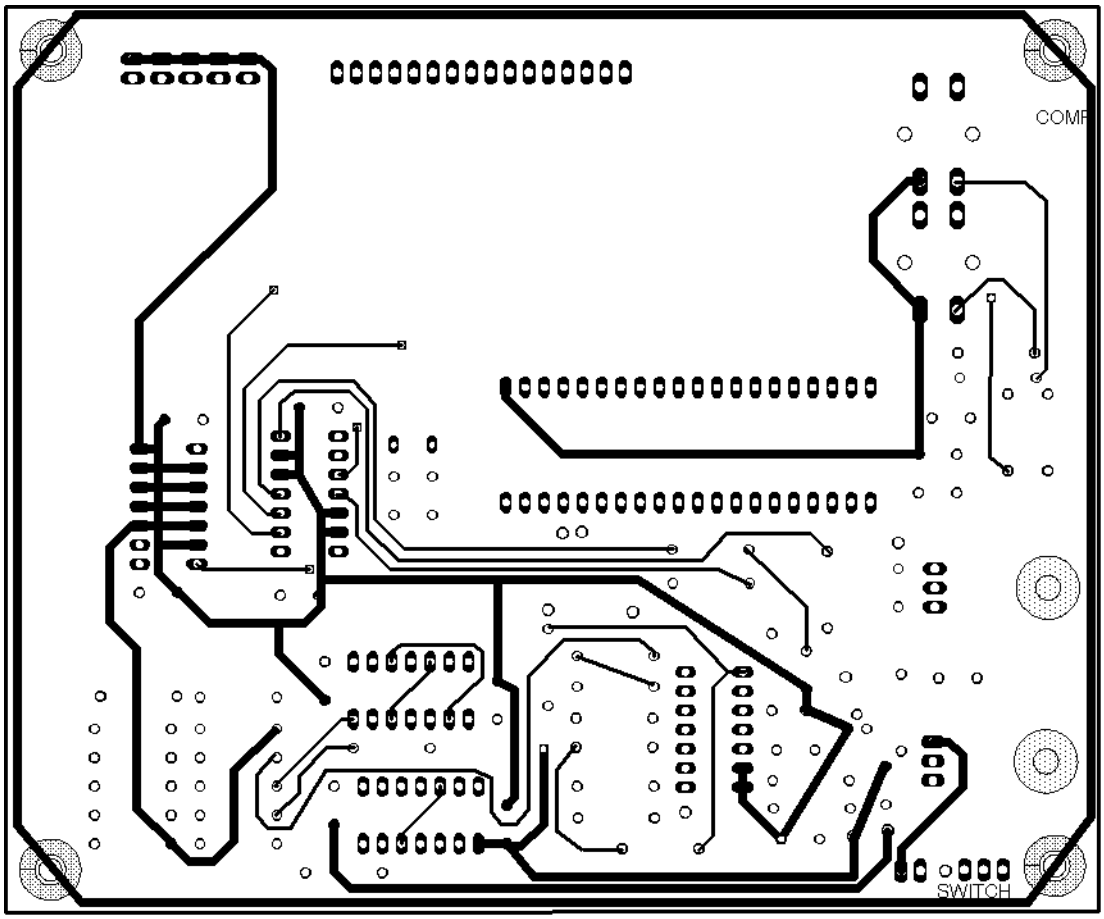

Fig. D.1 Component side of thoracic impedance simulator PCB.

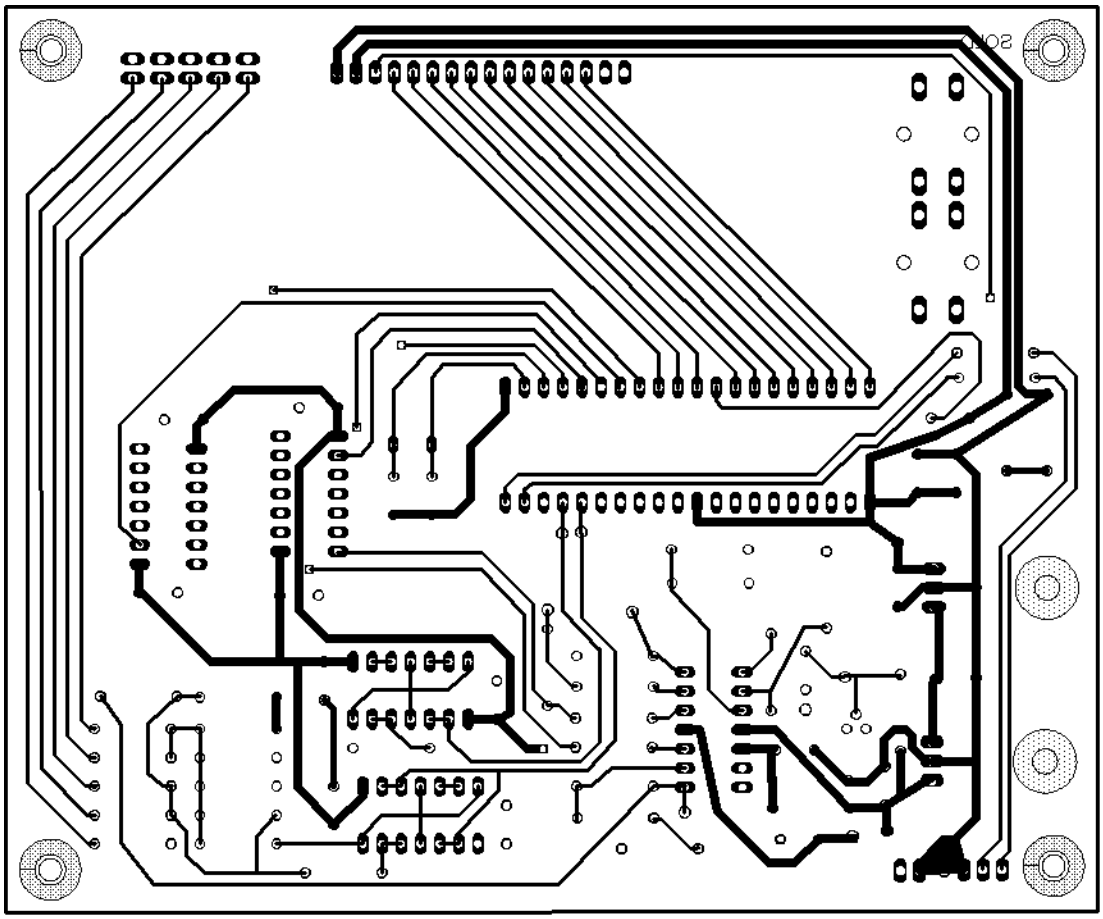

Fig. D.2 Solder side of thoracic impedance simulator PCB.

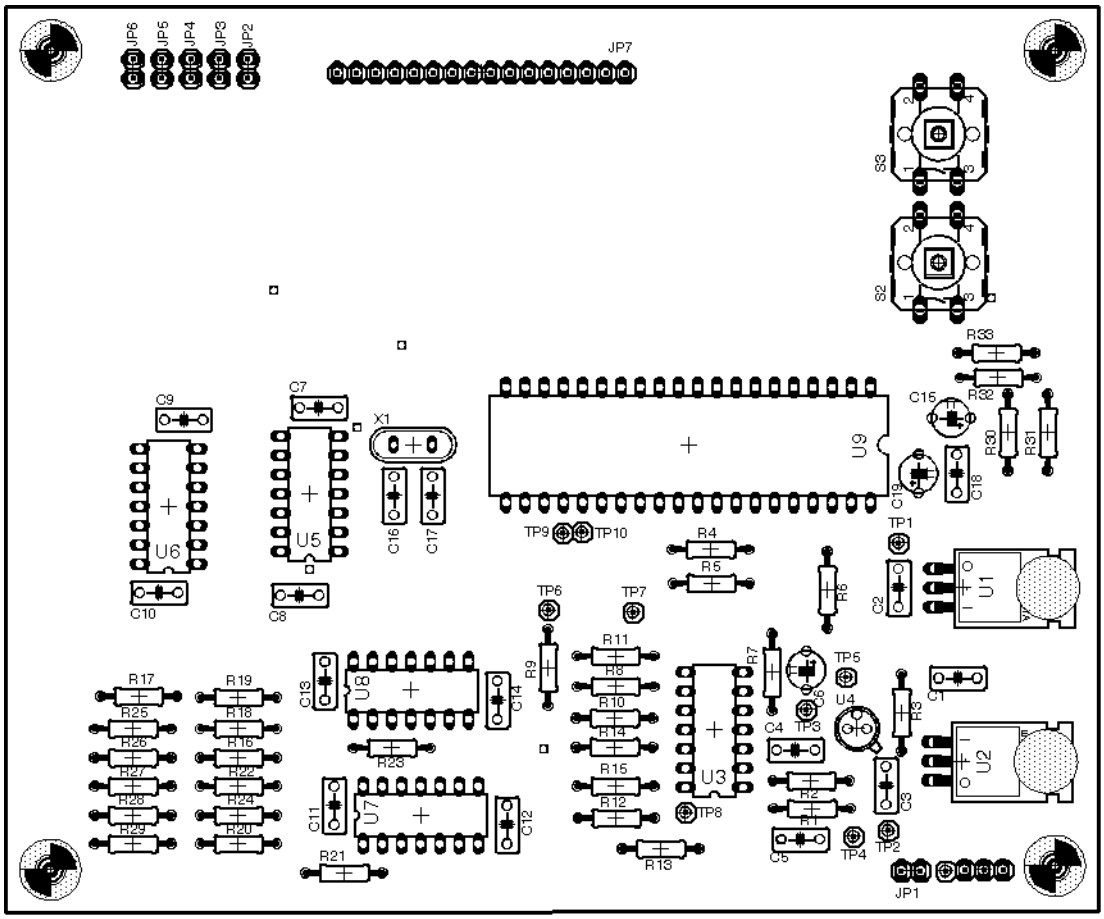

Fig. D.3 Component layout of thoracic impedance simulator PCB.

Appendix E

ENCLOSURE LAYOUT

Thoracic impedance simulator

Fig. E.1 Front panel of thoracic impedance simulator showing the on/off switch.

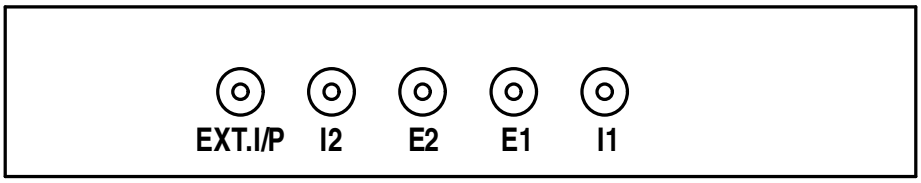

Fig. E.2 Rear panel of thoracic impedance simulator showing the five RCA connectors.

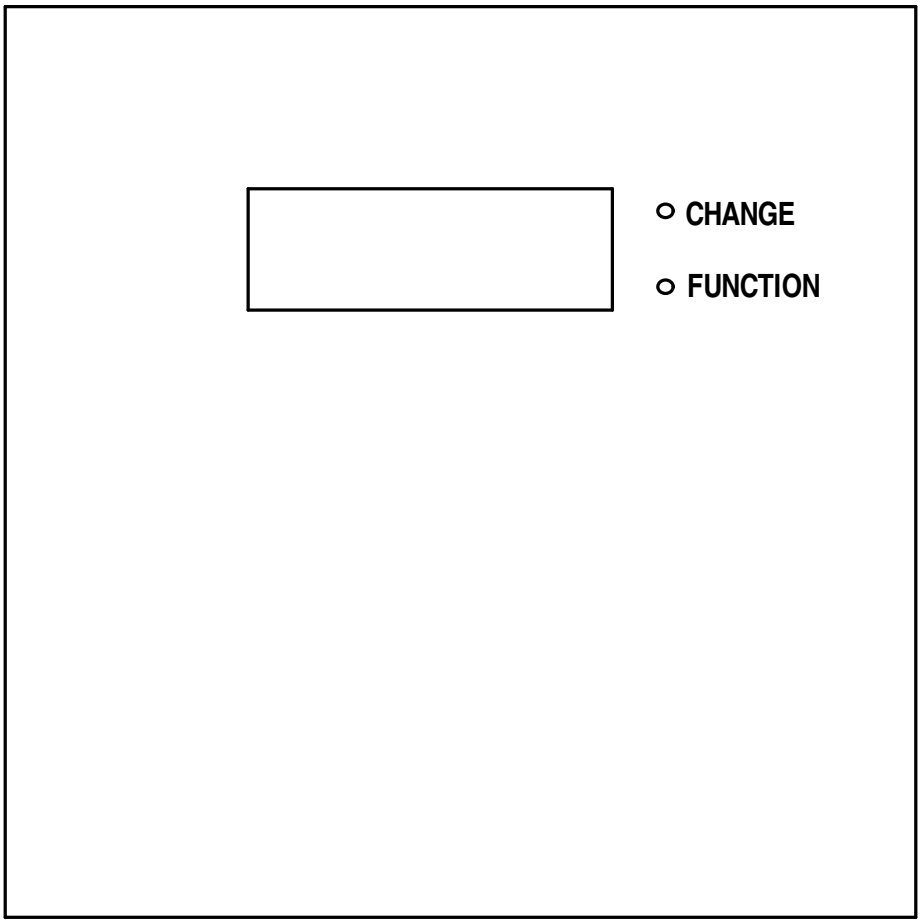

Fig. E.3 Top panel of thoracic impedance simulator showing the LCD and the two soft keys.

REFERENCES

[1] A. C. Guyton, *Textbook of Medical Physiology*, 7th ed., Philadelphia: Saunders, 1986.

[2] W. F. Ganong, *Review of Medical Physiology*, 13th ed., Connecticut: Prentice-Hall, 1987.

[3] "Cardiothoracic surgery," Keck School of Medicine of University of Southern California, http://www.cts.usc.edu/graphics/heart-crosssection1.jpg, downloaded on 17th July 2003.

[4] L. E. Baker, "Principles of the impedance technique," *IEEE Eng. Med. Biol. Mag.*, vol.8, pp. 11–15, Mar. 1989.

[5] R. P. Patterson, "Fundamentals of impedance cardiography," *IEEE Eng. Med. Biol. Mag.*, pp. 35–38, Mar. 1989.

[6] J. Malmivuo, and R. Plonsey, "Impedance plethysmography," in *Bioelectromagnetism*, 2nd ed., New york: Oxford Univ. Press, 1995.

[7] W. G. Kubicek *et al.*, "The Minnesota impedance cardiograph – theory and applications," *Biomedical Engineering*, vol. 9, pp. 410–416, Sept. 1974.

[8] B. B. Sramek, "Thoracic electrical bioimpedance: basic principle and physiologic relationship," *Noninvas. Cardiol.*, vol. 3, pp. 83–84, 1994.

[9] J. Vedru, "Electrical impedance methods for the measurement of stroke volume in man: state of art," *Acta et comm.*, Univ. Tartuensis, Tartu, Estonia, pp. 110–129, 1994.

[10] "CardioDynamics: the ICG company," CardioDynamics International Corporation, San Diego, CA, USA, http://www.cdic.com, downloaded on 18th July 2005.

[11] G. D. Jindal *et al.*, "Electrical impedance and photo plethysmography for medical applications," *BARC report*, *BARC/2004/E/025*, Sept. 2004.

[12] "MindWare Ambulatory Impedance Cardiograph," MindWare Technologies, Gahanna, Ohio, USA, http://www.mindwaretech.com/products_Imp.htm, downloaded on 20th July 2005.

[13] "Physio flow: noninvasive cardiac output," Manatec Biomedical, Paris, France, http://www.physioflow.com, downloaded on 20th July 2005.

[14] "IQ, minimizing emergent and acute care access," Wantagh Inc., Bristol, PA, UK, http://www.wantagh-inc.com/IQ/index.html, downloaded on 20th July 2005.

[15] "Hemo sapiens – complete noninvasive hemodynamics and O_2 transport dynamics at your fingertips." Hemo Sapiens Inc., AZ, USA, http://www.hemosapiens.com, downloaded on 20th July 2005.

[16] S. M. Joshi, "A cardiac output monitor," *B.Tech. Project report* (unpulished), Supervisor: P. C. Pandey, EE Dept., IIT Bombay,1993.

[17] S. M. Joshi, and P. C. Pandey, “A cardiac output monitor using impedance plethysmography,” in *Proc. Int. Conf. Rec. Adv. Biomed. Eng.*, (Osmania Univ. Hyderabad, India), Jan. 1994, pp. 157–160.

[18] K. S. Patwardhan, “An impedance cardiograph for stress testing,” *M.Tech. Dissertation* (unpublished),Supervisor: P. C. Pandey, EE Dept., IIT Bombay, Jan. 1997.

[19] B. Kuriakose, “An impedance cardiograph,” *M.Tech. Dissertation* (unpublished), Supervisor: P. C. Pandey, BME Group, IIT Bombay, Jan. 2000.

[20] N. S. Manigandan, “Development of hardware for impedance cardiography,” *M.Tech. Dissertation* (unpublished), Supervisor: P. C. Pandey, BME Group, IIT Bombay, July 2004.

[21] Y. Zhang, M. Qu., J. G. Webster, W. J. Tompkins, B. A. Ward, and D. R. Bassett, “Cardiac output monitoring by impedance cardiography during treadmill exercise,” *IEEE Trans. Biomed. Eng.*, vol. 33, pp. 1029–1041, Nov. 1986.

[22] M. Qu, Y. Zhang, J. G. Webster, and W. J. Tompkins, “Motion artifact from spot and band electrodes during impedance cardiography,” *IEEE Trans. Biomed. Eng.*, vol. 33, pp. 1029–1036, Nov. 1986.

[23] V. K. Pandey, “Signal processing for impedance cardiography,” *Ph.D. 2nd Progress Seminar Report* (unpublished), Supervisor: P. C. Pandey, BME Group, IIT Bombay, Aug. 2004.

[24] J. G. Webster, *Medical Instrumentation-Application and Design*, 3rd ed., New Delhi: John Wiley, 1998.

[25] H. G. Goovaerts, Th. J. C. Faes, E. Raaijmakers, and R. M. Heethaar, “An electrically isolated balanced wideband current source: basic considerations and design,” *Med. Biol. Eng.Comput.*, vol. 36, pp. 598–603, 1998.

[26] P. W. Van der Walt, “A Wein-bridge oscillator with high-amplitude stability,” *IEEE Trans. Instrum. Meas.*, vol. 30, pp. 292–294, 1981.

[27] E. Oxner, *Designing with Field - Effect Transistors*, 2nd ed., New York: McGraw-Hill, 1990.

[28] A. S. Sedra, and K. C. Smith, *Microelectronic circuits*, New York: CBS College Publishing, 1982.

[29] R. Mancini, and R. Palmer, “Sine-wave oscillator,” *Texas Instruments Application Report, SLOA060*, Mar. 2001.

[30] M. L. Meade, *Lock-in Amplifiers: Principles and Applications*, London: Peter Peregrinus, 1983.

[31] V. K. Pandey, N. S. Manigandan, and P. C. Pandey, “A tracking based drift cancellation circuit for biosignal acquisition,” in *Proc. Int. Conf. Instrumentation*, (Pune, India), Dec. 2004.

[32] V. K. Pandey, N. K. S. Naidu, and P. C. Pandey, “Tracking based baseline restoration for acquisition of impedance cardiogram and other biosignals,” accepted at *27th IEEE EMBS Annual Int. Conf.*, (Shanghai, China), Sept. 2005.

[33] N. S. Manigandan, V. K. Pandey, and P. C. Pandey, “Thoracic simulator for impedance cardiography”, *Proc. National Symposium on Instrumentation (NSI-28)*, (Pantnagar, India), Nov. 2003.

[34] J. M. Van de Water, *et al.*, “Impedance cardiography: the next vital sign technology?,” *Chest*, vol. 123, pp. 2028–2033, 2003.

[35] A. K. Deshpande *et al.*, “Impedance plethysmography of thoracic region: impedance cardiography”, *J. Postgrad. Med.*, vol. 36, pp. 207–212, 1990.

[36] G. B. Parulkar *et al.*, “Impedance cardiography in mitral valve disease,” *Indian Heart J.*, vol. 37, pp. 37–42, 1985.

[37] “HIC-2000 and HIC-3000 product information,” Bio-Impedance Technology Inc., Chapel Hill, NC, USA, http://www.microtronics-nc.com/BIT/HICProductInfo.html, downloaded on 20th July 2005.

[38] “IQ continuous non-invasive hemodynamic monitoring,” Wantagh Inc., Bristol, PA, UK, http://www.amethystinteractive.com/IQ, downloaded on 20th July 2005.